JACS
JOURNAL OF THE AMERICAN CHEMICAL SOCIETY
pubs.acs.org/JACS

Article

A Twist in Electronic Relaxation of Pyrimidine Nucleosides and Nucleotides: Impact of C5 Methylation on Nonadiabatic Transition and Photohydration Damage

Srijon Ghosh,[#] Yuki Obara,[#] Vishal Kumar Jaiswal,[#] Mario Taddei,[#] Artur Nenov, Irene Conti,* Marco Garavelli,* and Toshinori Suzuki*

Cite This: J. Am. Chem. Soc. 2026, 148, 18903−18918

Read Online

ACCESS | Metrics & More | Article Recommendations | Supporting Information

ABSTRACT: We report a combined experimental and theoretical study of the formation and decay dynamics of a ground-state twisted intermediate (TI) involved in the ultrafast internal conversion of UV-excited pyrimidine nucleosides and nucleotides in aqueous solution. Infrared transient absorption spectroscopy identifies a TI featuring a strongly twisted C5=C6 double bond, and its quantum yield (Φ_{TI}) and lifetime (τ_{TI}) are determined for structurally distinct nucleosides and nucleotides. Photohydration rates (k_{hyd}) measured under continuous 266 nm irradiation correlate directly with $\Phi_{TI} \times \tau_{TI}$, providing unambiguous evidence that the TI mediates the hydration reaction. Comparison of C5−H and C5−CH_3 derivatives reveals pronounced reductions in both Φ_{TI} and k_{hyd} upon methylation. Quantum mechanics/molecular mechanics dynamical simulations show that TI formation requires sufficient nuclear momentum along the TI-forming coordinate at the conical intersection, whereas vibrational energy randomization induced by C5 methylation and solvent interactions diminishes this momentum and consequently Φ_{TI}. The TI is neither diradical nor zwitterionic but instead contains an elongated, highly reactive C5=C6 double bond whose polarization and hydration reactivity are attenuated by C5 methylation. Consistently, the normalized reactivity index, $k_{hyd}/(\Phi_{TI} \times \tau_{TI})$, is substantially lower for C5-methylated compounds. A high activation barrier limits the photohydration quantum yield (~0.01), and τ_{TI} is primarily governed by isomerization back to the planar ground-state structure.

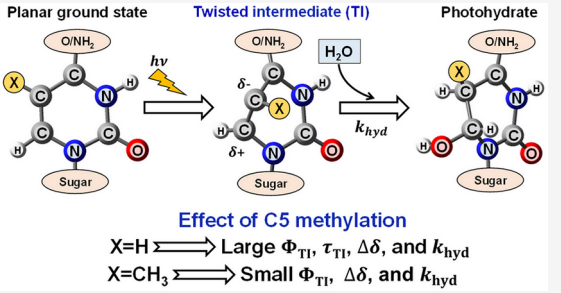

INTRODUCTION

The double helical structure of DNA, formed by adenine, thymine (Thy), guanine, and cytosine (Cyt), as proposed by Watson and Crick,[1] is essential for the storage and replication of genetic information. However, these nucleobases exhibit strong ultraviolet (UV) absorption bands around 260 nm and are consequently excited to the $^1\pi\pi^*$ states upon UV irradiation.[2−4] The formation of electronically excited states significantly increases the risk of photochemical reactions that can damage genetic material.[5−8] This raises a fundamental evolutionary question: why were nucleobases selected as the molecular medium for encoding genetic information during evolution? On modern Earth, the stratospheric ozone layer effectively blocks short-wavelength UV radiation from the Sun.[9] In contrast, the primitive Earth lacked a sufficient ozone shield, exposing the surface to a much higher level of UV radiation.[10] A compelling explanation is that all nucleobases undergo ultrafast electronic relaxation from their excited $^1\pi\pi^*$ states to the electronic ground state (S_0) via internal conversion, thereby dissipating the absorbed energy to the surroundings as heat and minimizing photodamage. This property underlies the concept of "photostability." Indeed, the fluorescence quantum yield (QY) for nucleobases in aqueous solution is extremely low,[3] and it is well-known that their excited $^1\pi\pi^*$ states are rapidly quenched via radiationless transitions to either S_0 or a dark (nonfluorescent) state. Its mechanistic detail has been the subject of extensive spectroscopic and theoretical investigation.[2−4,11−42]

In their seminal study reported two decades ago, Kohler and colleagues[14] investigated the relaxation dynamics of nucleobases, nucleosides, and nucleotides in aqueous solution using UV−vis transient absorption spectroscopy (TAS). By monitoring the TA signal at 570 nm, they confirmed that the $^1\pi\pi^*$ states of these molecules decay in less than one picosecond. The TA signal at 250 nm revealed ground-state bleach recovery (GSBR), which included both a fast component (within several ps) and a slow component with time constants ranging from tens to hundreds of picoseconds in pyrimidine

Received: January 11, 2026
Revised: April 15, 2026
Accepted: April 20, 2026
Published: May 4, 2026

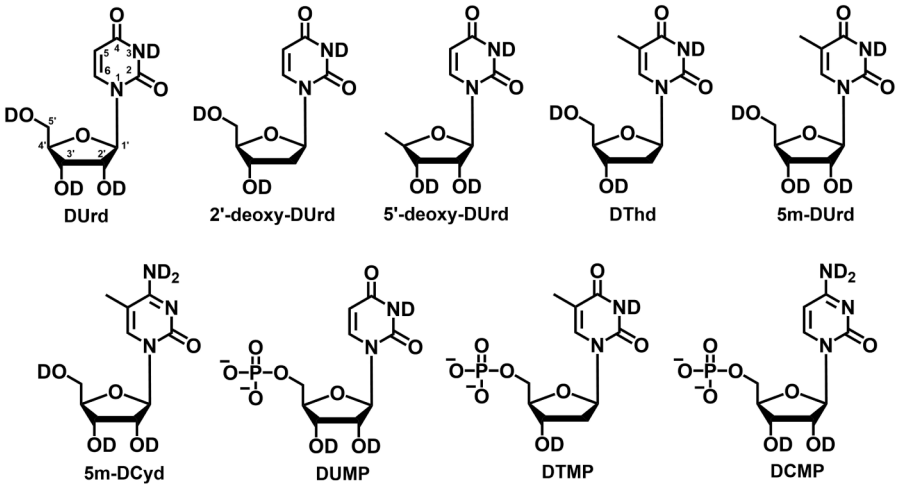

Figure 1. Molecular structures of DUrd (tetradeuteriouridine), 2′-deoxy-DUrd (tetradeuterio-2′-deoxyuridine), 5′-deoxy-DUrd (trideuterio-5′-deoxyuridine), DThd (trideuteriothymidine), 5m-DUrd (tetradeuterio-5-methyluridine), 5m-DCyd (pentadeuterio-5-methylcytidine), DUMP (trideuteriouridine-5′-monophosphate), DTMP (dideuteriothymidine-5′-monophosphate), and DCMP (tetradeuteriocytidine-5′-monophosphate). DThd and DTMP are deoxyribose derivatives by default. The symbol "D" is used to indicate molecules that have undergone H/D exchange in D_2O.

nucleobases, while no such slow relaxation was observed in purine bases. Remarkably, the slower component accounted for 40−50% of the total relaxation in some pyrimidine nucleosides and nucleotides. Additionally, the TA signal at 340 nm showed decay rates that matched the rates for the aforementioned GSBR. These findings led Kohler and colleagues to assign the slow recovery to the cascaded internal conversion process $^1\pi\pi^* \rightarrow {}^1n\pi^* \rightarrow S_0$. Subsequent studies adopted the same interpretation, and theoretical calculations supported the presence of the two relaxation pathways.[4] This two-step internal conversion model has been widely accepted, although questions have remained. For example, it was unclear why the QY for $^1n\pi^*$ could be as high as 0.4−0.5 despite destabilization of the $^1n\pi^*$ state in an aqueous environment.

Miura et al.[27] used extreme ultraviolet time-resolved photoelectron spectroscopy (EUV-TRPES) to examine the nonadiabatic electronic dynamics in gaseous and aqueous nucleobases and their derivatives. Photoionization using high-energy EUV photons (>20 eV) enabled detection of multiple excited state species regardless of the electronic configuration and spin multiplicity, shedding new light on "dark" states that are almost undetectable using other optical methods. The EUV-TRPES experiments on aqueous pyrimidine nucleobase derivatives unequivocally showed that the QY for the $^1n\pi^*$ state is far too low to account for the aforementioned slow relaxation processes. A low QY for the $^1n\pi^*$ state was also pointed out for aqueous uridine (Urd) by Borrego-Varillas et al.[24] Subsequently, via vibrational fingerprinting using infrared TAS (IR-TAS), Obara et al.[43,44] identified the metastable species to be a ground-state intermediate with a highly twisted C5=C6 double bond: its presence has been theoretically predicted by Park et al.[41] IR-TAS identified the formation of twisted intermediates (TIs) for all pyrimidine nucleobases upon UV excitation.[43,44] While an earlier IR spectroscopic study by Pilles et al.[17] also suggested the formation of a transient species other than the $^1n\pi^*$ state for aqueous Thy derivatives, definitive assignment was lacking. All experimental evidence obtained from UV−vis TAS, EUV-TRPES, IR-TAS, together with quantum chemical calculations, has therefore converged to support a novel mechanism for the electronic relaxation of these building blocks of life. The twisted structure lies at a shallow local minimum in the S_0 potential energy surface located at an energy more than 80 kcal/mol higher than the global minimum for the planar structure.[26,41,43,44] An energy barrier separates the two minima, allowing a relatively long lifetime for the intermediate.

On the other hand, UV irradiation induces photochemical reactions of nucleobases, nucleosides, and nucleotides in aqueous solution. The mechanism has been studied since the 1960s, but is yet unresolved: Fisher and Johns published an excellent review of studies up to the early 1970s.[45] It has been shown that the reaction rate does not decrease at low concentration,[46] indicating that the reaction does not primarily involve cyclobutane pyrimidine dimer formation. The kinetic isotope effect in HDO or D_2O indicated that it is a hydration reaction, and mass spectrometry and nuclear magnetic resonance (NMR) studies have firmly identified the hydrates as products.[47,48] Interestingly, the C6-oxygenated product was found to be preferentially produced over a C5 counterpart.[49,50] Because this reaction does not occur without photoexcitation, it must occur in electronically excited states or highly vibrationally excited states in S_0.[45] The triplet state was excluded because the reaction occurred even in the presence of triplet quenchers. As mentioned earlier, EUV-TRPES has unequivocally established that the QY for the $^1n\pi^*$ is extremely low.[27] Recent quantum chemical calculations predicted very high potential barriers for the hydration reactions in the S_1 and S_2 states of uracil (Ura) and Thy,[51] ruling out their involvement. Early studies have indicated that preferential OH insertion at C6 is consistent with a partial positive charge at C6 in the ground state, suggesting a ground-state reaction.[45] (It is noted that this argument in the literature is not rigorous, because the twisted structure must be considered, as discussed in the present paper.) Park et al.[41] proposed a mechanism via the aforementioned TI in S_0, in which the reaction barrier was estimated to be 7−9 kcal/mol. Based on the identification of the TI by Obara et al.,[43,44] in the present study we performed a detailed investigation of the hydration reaction involving the TI.

https://doi.org/10.1021/jacs.6c00684
J. Am. Chem. Soc. 2026, 148, 18903−18918

Table 1. Summary of GSBR Fitting Results Assuming Single Exponential Decay for Twisted Intermediate in Aqueous (D_2O) Solution

Sample	τ_ν	τ_{TI}^{eff}	τ_{trp}	Φ_ν	Φ_{TI}	Φ_{trp}
DUrd	5.7 ± 0.2	334 ± 7	>3600	0.46	0.45	0.09
DUMP	5.6 ± 0.2	350 ± 5	>3600	0.40	0.50	0.10
2′-deoxy-DUrd	8.9 ± 0.4	327 ± 7	>3600	0.38	0.52	0.10
5′-deoxy-DUrd	7.1 ± 0.2	368 ± 6	>3600	0.4	0.49	0.10
DThd	3.2 ± 0.1	813 ± 50	>3600	0.85	0.08	0.06
DTMP	2.6 ± 0.1	1177 ± 95	>3600	0.92	0.05	0.03
5m-DUrd	2.4 ± 0.1	616 ± 21	>3600	0.83	0.11	0.05
DCyd[44]	3.3 ± 0.1	43.8 ± 0.3	>3600	0.72	0.25	0.03
5m-DCyd[a]	6.3 ± 0.1	122 ± 10	>3600	0.90	0.06	0.04
DCMP	2.5 ± 0.1	51 ± 1	>3600	0.75	0.22	0.03

[a]GSBR was obtained from the analysis described in Supporting Information Section F(e).

Due to the extremely low QY (10^{-3}–10^{-2}) for the hydration reaction, real-time observation of the hydration reaction using EUV-TRPES or IR-TAS is challenging. On the other hand, it is possible to examine the correlation of the QY (Φ_{TI}) and lifetime (τ_{TI}) of the TI with the hydration reaction rate (k_{hyd}). It has been reported that k_{hyd} is ten times higher for uridine (Urd) than for Ura,[49] which is qualitatively consistent with the higher Φ_{TI} for the TI in Urd.[43] However, a quantitative analysis has been lacking regarding the correlation between the generation of the TI and the hydration reaction. Thus, we performed comprehensive IR-TAS and hydration reaction experiments for aqueous nucleosides and nucleotides and examined the relationship among the molecular structure, Φ_{TI} and τ_{TI}, and the hydration reactivity. The results indicate that τ_{TI} is more important than Φ_{TI} with regard to explaining the difference between Ura and Urd.

To understand the mechanistic details of photochemical processes, dynamical simulations based on accurate electronic structure calculations are indispensable. Studies have already been reported by several research groups on nuclear dynamics under both isolated conditions in the gas phase and in aqueous solution, from the Franck–Condon region on the excited state potential energy surfaces to the conical intersections mediating the internal conversion to the ground state.[23,24,32,39,40,51,52] However, the analysis so far is lacking with regard to the dynamics after passing through the conical intersection. The key question concerns the bifurcation of the dynamics into trapping in the TI and direct relaxation to the planar global minimum in S_0. This bifurcation is decisive for the subsequent hydration reactivity via the TI. To address this question, we carried out mixed quantum-classical molecular dynamics simulations for three pyrimidine nucleosides within a quantum mechanics/molecular mechanics (QM/MM) framework using an explicit water solvent model employing the surface hopping algorithm. We also performed a detailed analysis of the electronic structure of the TI to illuminate the factors dictating the different hydration reaction rates observed for the nucleosides Urd, thymidine (Thd), and cytidine (Cyd). The experimental and theoretical results presented here provide a foundation for understanding the photophysics and photochemistry of canonical and epigenetically modified nucleosides such as 5-methylated cytidine (5m-Cyd). The structures of the molecules discussed in the present paper are illustrated in Figure 1. Because a phosphate-buffered D_2O (PB-D_2O) solution was employed in the IR-TAS measurements, D/H exchange occurred. These structures were confirmed by NMR spectroscopy (Supporting Information Section C).

EXPERIMENTAL METHODS

Infrared Transient Absorption Spectroscopy

The experimental setup and procedures for IR-TAS used in this study are described in our previous publication.[43] Further technical details, such as experimental conditions, are summarized in the Supporting Information. IR-TAS was carried out using a Ti:sapphire regenerative amplifier system (35 fs, 800 nm, 10 kHz), which pumped two optical parametric amplifiers to generate independently tunable 267 nm UV pump and 5–10 μm IR probe pulses. To minimize coherent artifacts, the UV pump pulse was temporally stretched to approximately 0.6 ps. A mechanical delay stage controlled the pump–probe timing, and a magic angle configuration was used to eliminate rotational anisotropy. Sample solutions were prepared in 50 mM phosphate-buffered D_2O (pH ≈ 6.8) and circulated through a custom-built flow cell with CaF_2 windows and PTFE spacers, yielding an optical path length of 0.05 mm. The IR signals were detected using a grating monochromator and a 64-channel mercury cadmium telluride array. The IR absorption spectrum of the solvent was independently recorded using a Fourier-transform infrared (FTIR) spectrometer equipped with temperature control, allowing correction for solvent heating effects in the transient spectra. Additional details, including excitation parameters and purities of chemicals are provided in Supporting Information Sections A and B. The solvent heating effect grows in the first 10 ps and then remains constant. This time-dependent amplitude is modeled by the following equation:[43]

$$A_t^{Solv.} = A_\infty^{Solv.}\left(1 - e^{-\frac{t}{\bar{\tau}}}\right) \quad (1)$$

where $A_\infty^{Solv.}$ is obtained from temperature-dependent FTIR spectra. $\bar{\tau}$ is the average of τ_ν which is the smallest GSBR time constant obtained from the IR-TAS measurements (Table 1).

The population of each species was determined from the GSBR time profile to avoid errors arising from species-dependent IR absorbance. For spectroscopic analysis, we performed global fitting of spectra in the long-delay-time region, where vibrational relaxation is complete (>10 ps), and we determined the decay associated difference spectrum (DADS) using GloTarAn (version 1.5.1).[53] For 5m-DCyd, as the lifetime of the $^1\pi\pi^*$ state is considerably longer than other cases,[18] we used a slightly different analysis as discussed later. Because the IR-TA spectra clearly indicated the formation of a triplet state and a TI in the long-delay-time region, the time-dependent IR-TAS data, $S(\nu, t)$, are expressed as

$$S(\nu, t) = \sum_{n=1}^{2} \mathrm{DAD}_n(\nu) \exp\left[-\frac{t}{\tau_n}\right] + \delta(\nu) \quad (2)$$

https://doi.org/10.1021/jacs.6c00684
J. Am. Chem. Soc. 2026, 148, 18903–18918

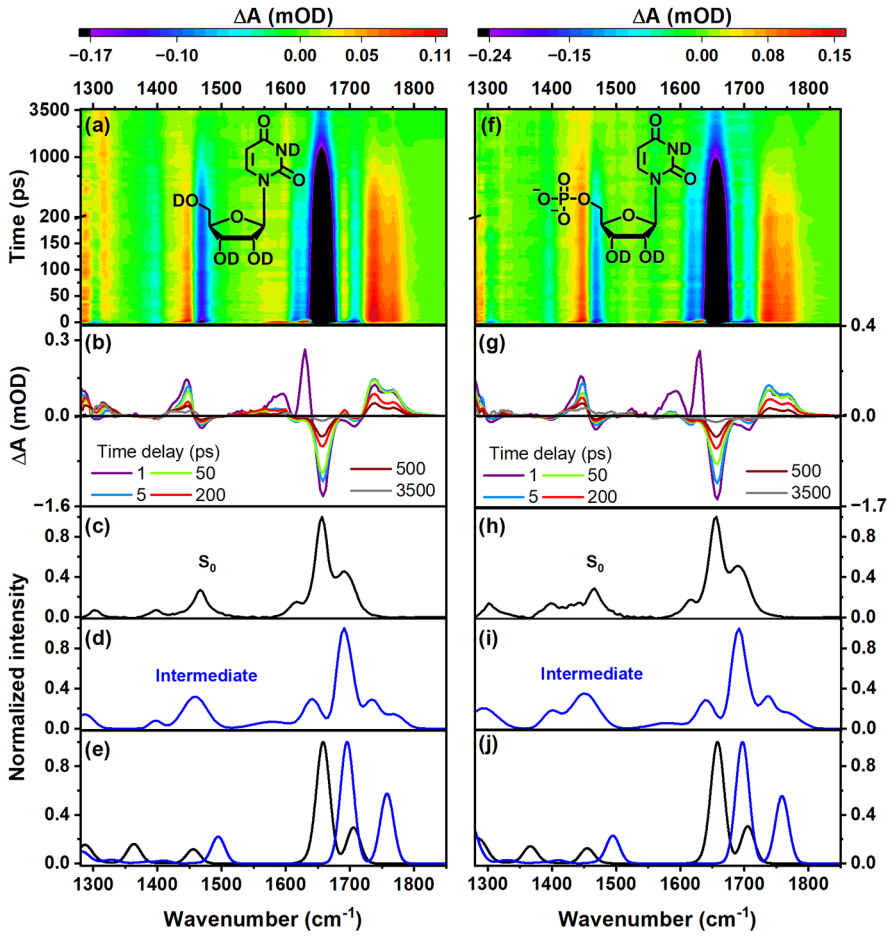

Figure 2. IR-TA spectra measured under 267 nm photoexcitation (a and f), selected lineouts (b and g), static IR spectrum measured for S_0 (c and h), IR spectrum of intermediate species (d and i), and theoretical IR spectra of global minimum (S_0) and TI (e and j), for DUrd and DUMP in PB-D_2O (20 mM), respectively. In (e) and (j), the theoretical calculations were performed using a harmonic model and DFT at the B3LYP/def2-TZVP+PCM(D_2O) level of theory, assuming the *anti*-rotamer. The calculated frequencies were scaled and stick spectra were convoluted with a Gaussian function, as detailed in Supporting Information Section D(a) and summarized in Table S3.

where $DAD_n(\nu)$ and τ_n are the DADS and the lifetime of the n^{th} component, and $\delta(\nu)$ is the residual (noise). $DAD_n(\nu)$ can be expressed in terms of the ground-state IR spectrum, $GS(\nu)$, of unexcited molecules and the species associated spectrum (SAS) of the n^{th} component, $SAS_n(\nu)$:

$$DAD_n(\nu) = -c_{gs}^n GS(\nu) + SAS_n(\nu) \quad (3)$$

where c_{gs}^n is an expansion coefficient. To determine $SAS_n(\nu)$, we performed least-squares fitting of $DAD_n(\nu)$ using $GS(\nu)$ and Gaussian functions that are constrained to be positive. $SAS_n(\nu)$ is thus expressed as a linear combination of Gaussian functions.

Photodegradation Measurements

For measurements of the hydration reaction, a 266 nm continuous-wave laser (Oxide Corp. FQ-1100B) was used as the light source. The output power was adjusted to 15 mW, and the beam was expanded to obtain an effective incident photon flux of 1.88×10^{18} photons·cm^{-2}·min^{-1}. The initial absorbance at 266 nm was adjusted to approximately 0.40 to satisfy the isoabsorptivity condition, ensuring that all samples absorbed nearly the same number of photons. The sample solution was continuously circulated through a quartz cell, and UV absorption spectra were measured consecutively with a certain time interval. The peak absorbance is directly proportional to the concentration. The primary pathway for photodegradation is photohydration,[45] for which pseudo-first-order kinetics[49] can be assumed with a rate equation given by

$$\ln(C_t/C_o) = -k_{obs}t \quad (4)$$

where C_t is the concentration at time t. A plot of $\ln(C_t/C_o)$ versus t yields a straight line whose slope gives the rate constant (k_{obs}). Deionized H_2O was used as a solvent and the room temperature was around 295 K. The details of the calculation for the true photohydration rate constant (k_{hyd}) and the photohydration quantum yield (Φ_{hyd}) are described in Supporting Information Section E.

COMPUTATIONAL METHODS

Simulation of IR Spectra

The experimentally observed IR spectrum at room temperature represents an ensemble average over many possible solute−solvent configurations. Ideally, IR spectra should be predicted using QM/MM calculations, as we previously demonstrated for DUra.[43] However, QM/MM calculations are computationally highly demanding, and their application to the TI proved to be both technically and computationally challenging.

As an alternative, we calculated the IR spectra using density functional theory (DFT) at the B3LYP/def2-TZVP level,[54,55] as implemented in the Gaussian 16 program package.[56] Harmonic vibrational frequency calculations were performed in combination with the polarizable continuum model (PCM).[56] To account for hydrogen-bonding interactions between the solute and solvent, several explicit water molecules were included in the quantum chemical calculations in selected cases. For Cyt derivatives, inclusion of a certain number of explicit D_2O molecules improved the agreement

https://doi.org/10.1021/jacs.6c00684
J. Am. Chem. Soc. 2026, 148, 18903−18918

with the experimental spectra,[57] particularly where strong and specific hydrogen-bonding interactions were expected to influence vibrational frequencies.

However, this approach does not account for ensemble averaging over solvation structures but instead provides the IR spectrum corresponding to the optimized geometry at effectively zero temperature. Consequently, inclusion of a larger number of explicit water molecules does not necessarily improve the agreement with the experimental results. Rather, the level of agreement depends on the diversity of solvation structures in solution and must therefore be evaluated on a case-by-case basis. To illustrate this dependence, Supporting Information Section D(a) presents IR spectra calculated using varying numbers of explicit water molecules.

IR absorption spectra were computed for DUrd, 2′-deoxy-DUrd, 5′-deoxy-DUrd, DUMP, DThd, 5m-DUrd, DTMP, 5m-DCyd, and DCMP. For each system, calculations were performed for both the planar global minimum and the TI in the S_0 state. Spectra were also calculated for both *syn*- and *anti*-rotamers. As shown in Supporting Information Section D(b), the IR spectra of the *syn*- and *anti*-conformers are very similar. Because previous NMR studies[58] have indicated that the *anti*-form predominates in solution, only the IR spectra for the *anti*-conformers are considered herein.

Simulation of Nonadiabatic Dynamics

The photoinduced nonadiabatic dynamics were simulated at the XMS-CASPT2 level with the fewest switches using the Tully surface-hopping algorithm with the Tully−Hammes−Schiffer scheme[59] including decoherence correction.[60] Only trajectories that decayed to the ground state within the simulation time were considered, resulting in 43 trajectories for Urd (*syn*-conformer), 44 for Thd, and 41 for Cyd (*anti*-conformers for both). A time step of 0.5 fs was utilized for the surface-hopping dynamics simulations. These nonadiabatic simulations were conducted by interfacing the COBRAMM[61] QM software (OpenMolcas[62] /Gaussian16[56]) with the MM software (Amber[63]). Each trajectory was propagated for at least 300 fs after the hop to allow relaxation and to ensure that any twisted conformations corresponded to dynamically stable minima. The protocol for producing the optimized QM/MM setup (Figure S20) from classical molecular dynamics and further details on surface-hopping dynamics have been previously described.[24] The time-derivative coupling between two electronic states was computed following the Tully−Hammes−Schiffer scheme using the overlap integrals between the adiabatic wave functions at successive time steps. The overlap integrals were computed using the RASSI module available in OpenMolcas.[62] The XMS-CASPT2 computations were performed using a CASSCF reference wave function averaged over 9 states. The active space included 14 electrons in 10 orbitals consisting of the full valence π/π^* orbitals as well as the oxygen and nitrogen lone pairs (Figure S21).

The S_0 potential energy surface connecting the two stable minima was explored through static calculations at the RMS-CASPT2 level of theory. A reduced active space of six electrons in six orbitals (6,6) (Figure S22) was sufficient to accurately capture the electronic structure along this pathway, which was verified by comparing the results obtained with higher-level active spaces (Figure S23). The planar and TI minima, as well as the transition state connecting them, were optimized at this level of theory averaged over 2 states. All CASPT2 computations were performed with an IPEA shift of 0.0 and an imaginary shift of 0.2, using the ANO-L-VDZP basis set throughout. Multiwfn[64,65] was used to calculate the Merz−Kollman charges fitted to the electron density for the ground-state wave function.

RESULTS

IR-TAS

Uracil Derivatives. Figure 2a,b shows a two-dimensional (2D) map of IR-TA spectra and representative IR spectra measured at selected time delays. Figure 2c is the steady-state IR spectrum of DUrd in PB-D_2O. The IR-TA spectra display negative (blue) ground-state bleach (GSB) signals at 1658 and 1692 cm^{-1}, corresponding to out-of-phase and in-phase C=O stretching vibrations, respectively. Additional GSBs are also evident, especially around 1466 cm^{-1}, corresponding to C−N stretching vibrations of the pyrimidine ring. At pump−probe delay times <10 ps, vibrational relaxation induces a rapid blue-shift of the IR bands for vibrationally excited molecules generated by ultrafast internal conversion to S_0. The vibrational relaxation is completed within 10 ps, and spectral evolution becomes considerably slower thereafter. The C=O stretching bands (positive) seen at 1691 and 1739 cm^{-1}, blue-shifted with respect to the values prior to photoexcitation, are the fingerprints of the TI, as discussed previously.[43] Additionally seen is a positive signal near 1445 cm^{-1}, which corresponds to C=C stretching vibrations of the TI. Weak signals extending beyond 1 ns are due to the triplet state. We extracted the SAS of the TI, as shown in Figure 2d, by performing global fitting of the IR-TAS data beyond 10 ps, assuming a TI and a triplet species. Harmonic frequency calculations for the TI of DUrd at the B3LYP/def2-TZVP level with PCM (D_2O) solvation (Figure 2e) confirmed its assignment.

Preliminary IR-TAS results for DUrd have been reported in our previous paper,[43] in which we showed that GSBR occurs with dual time constants of 63(5) ps and 528(19) ps. Whether TI decay can be expressed using a single or dual exponential function is interesting, as nucleosides take a variety of conformers. The pyrimidine nucleosides have structural isomers at least in terms of the rotational angle of the N-glycosidic bond, puckering of the 5-membered ribose group, and 4′-5′ bond rotation. For the former, the *anti*-configuration, where the carbonyl group at C2 is pointing away from the ribose group, is dominant (∼95%).[58] For the latter, the C3′-endo and C2′-endo are thermally populated at a nearly equal ratio (in deoxyribose, the C2′-endo is populated slightly more). To investigate the decay dynamics of the TI more closely, we examined both the GSBR and the decay waveforms for C=O stretching of the TI. In Table 1, we list the lifetime of the TI obtained assuming a single exponential decay. We define this time constant as the effective lifetime (τ_{TI}^{eff}) of the TI (averaged over possible isomers), and we use τ_{TI}^{eff} to analyze the hydration reaction rate in a later section.

Figure 3a shows the GSBR waveforms at 1658 cm^{-1} measured for DUrd along with the results of least-squares fitting using a single (blue) or dual (pink) exponential decay function for the intermediate: the dual exponential decay function provided a superior fit. Direct relaxation to the planar minimum followed by vibrational relaxation, as well as relaxation mediated by the triplet state, were considered, with lifetimes τ_v and τ_{trp}, respectively. The best-fit time constants for the GSBR were 3.9 (0.1) ps, 85(1) ps, 738(15) ps, and >3600 ps, as listed in Table 2. The two time constants between 10−1000 ps are attributed to TIs. The Φ_{TI} in Table 1 and $\Phi_{TI}^1 + \Phi_{TI}^2$ in Table 2 are very similar. To examine the influence of OH groups on the decay dynamics, we measured the IR-TA spectra of TIs for 2′-deoxy-DUrd and 5′-deoxy-DUrd, as shown in Supporting Information Section F(a). The overall spectral features are very similar to those for DUrd, and only the GSBR waveforms are shown in Figure 3b and c, respectively. In both cases, the dual exponential decay function provides better fits than the single exponential decay function. The extracted time components are similar to those for DUrd, indicating that −OH substitution in the ribose has a minimal

https://doi.org/10.1021/jacs.6c00684
J. Am. Chem. Soc. 2026, 148, 18903−18918

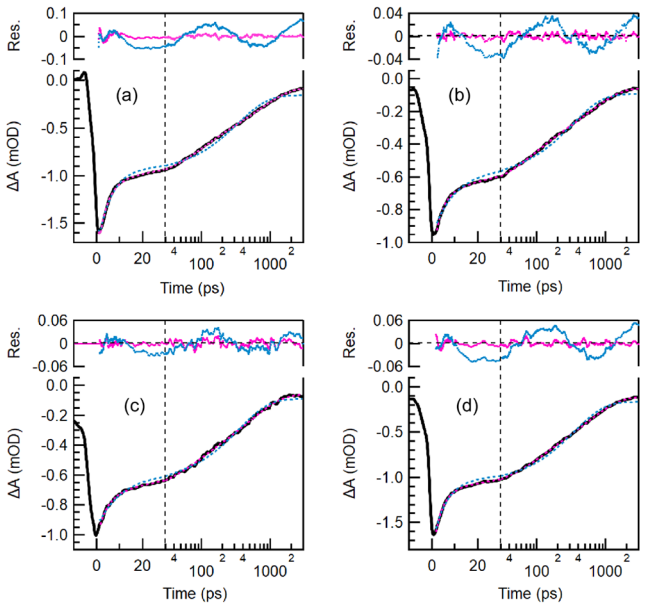

Figure 3. GSBR waveforms at 1658 cm^{-1} (black solid line) and their exponential fits for (a) DUrd, (b) 2′-deoxy-DUrd, (c) 5′-deoxy-DUrd, and (d) DUMP. Blue and pink dashed lines show least-squares fitting results assuming a single and dual exponential decay for the intermediate, respectively, in addition to direct internal conversion to S_0 and cascaded relaxation via the triplet state. The waveforms exhibit complex features in the negative time range due to free induction decay in the probe-pump pulse sequence. The horizontal scale is linear up to 30 ps and logarithmic thereafter.

influence on the dynamics. Both Φ_{TI} and τ_{TI}^{eff} for DUrd (Table 1) are greater than those (0.35 and 30 ps, respectively) for DUra,[43] indicating a strong influence of the ribose group, especially on τ_{TI}^{eff}. The waveform and the fitting results at the positive marker band for the TI for DUrd are shown in Supporting Information Section F(c). Global fitting results assuming two decay components for the TI for DUrd, and the feasibility of identifying two structural isomers are also discussed in Supporting Information Section F(d).

Figure 2f–h shows a 2D map of the IR-TA spectra, IR spectra at selected time delays, and steady-state IR spectra of DUMP in PB-D_2O, respectively. The spectral features are similar to those for DUrd. More precisely, the best-fit waveform for GSBR (Figure 3d) exhibits dual time constants of 88 (2) ps and 596(7) ps, consistent with the results for DUrd (Table 2), demonstrating that the phosphate group has only a minor influence on the dynamics. The SAS of the intermediate (Figure 2i) displays blue-shifted C=O stretching bands, the marker of the TI, in agreement with the calculated spectrum (Figure 2j). The Φ_{TI} and τ_{TI}^{eff} determined in the present study are in reasonable agreement with those previously reported by Hare et al.[14] and Brister and Crespo-Hernández,[66] when their assignment is corrected from the $^1n\pi^*$ state to the TI.

Thymine Derivatives. Figure 4a–c shows a 2D map of the IR-TA spectra, lineouts at selected time delays, and the steady-state IR spectrum of DThd in PB-D_2O, respectively. In the IR-TA spectrum, negative (blue) GSB signals are observed for the C=O stretching bands at 1664 and 1692 cm^{-1}. Global fitting delineates the IR absorption spectrum (Figure 4d) of TI with characteristic blue-shifted C=O stretching bands at 1681 and 1739 cm^{-1}, consistent with quantum chemical calculations (Figure 4e). Least squares fitting of GSBR (Figure 5a) assuming a single exponential decay for TI yields Φ_{TI} and τ_{TI}^{eff} values of 0.08 and 813(50) ps (Table 1). Possibly due to the low Φ_{TI}, least-squares fitting assuming a single exponential decay provided a reasonable fit.

5m-DUrd is structurally almost identical to DThd, except that the hydroxyl group at the 2′ position is missing. Thus, it is interesting to compare the dynamics of these two molecules. Detailed IR-TA results are shown in Supporting Information Section F(e). The presence of a TI with blue-shifted IR absorption bands was confirmed. The GSBR waveform is shown in Figure S12. Assuming a single exponential decay for TI yields a τ_{TI}^{eff} value of 616(21) ps and a Φ_{TI} value of 0.11.

A 2D map of the IR-TA spectra, selected IR spectra, and the steady-state IR spectrum of DTMP in PB-D_2O are shown in Figure 4f–h, respectively. Blue-shifted IR absorption bands are evident for the TI (Figure 4i), consistent with the quantum chemical calculations (Figure 4j), indicating only a minor influence of the phosphate group. Both the spectral characteristics and kinetic behavior are consistent with an earlier report by Pilles et al.,[17] although the QY values differ slightly, most probably due to the difference in the analysis method (global fitting vs GSBR fitting). Overall, DThd and DTMP exhibit remarkably similar dynamics, with comparable Φ_{TI} and τ_{TI}^{eff} values (Table 1).

Cytosine Derivatives. We have previously reported that the IR-TAS of DCyd exhibits a marker band at ∼1580 cm^{-1} associated with the TI.[44] Figure 6a–c presents a 2D map of IR-TA spectra, selected lineouts, and the steady-state IR spectrum of DCMP in PB-D_2O, respectively. In the post-10 ps region, where vibrational relaxation has completed, two components were identified. GSBR fitting reveals that the dominant contribution arises from a TI with a τ_{TI}^{eff} of 51 ps and a Φ_{TI} of 0.22 (Table 1), which is responsible for the 1580 cm^{-1} band (Figure 6d) in agreement with calculations (Figure 6e). The dual decay function provides a slightly superior fit to the GSBR waveform (Figure S13a), although the time constants for the two components are quite close to each other. The common

Table 2. Summary of GSBR Fitting Results for Uracil and Cytosine Derivatives Assuming Dual Exponential Decay for Twisted Intermediate in Aqueous (D_2O) Solution

Sample	τ_v	τ_{TI}^1	τ_{TI}^2	τ_{trp}	Φ_v	Φ_{TI}^1	Φ_{TI}^2	Φ_{trp}
DUrd	3.9 ± 0.1	85 ± 1	738 ± 15	>3600	0.42	0.22	0.31	0.04
DUMP	3.5 ± 0.1	88 ± 2	596 ± 7	>3600	0.41	0.19	0.34	0.06
2′-deoxy-DUrd	3.6 ± 0.1	73 ± 1	623 ± 8	>3600	0.37	0.25	0.33	0.05
5′-deoxy-DUrd	4.1 ± 0.1	70 ± 2	594 ± 8	>3600	0.36	0.20	0.37	0.07
DCMP	2.3 ± 0.1	23 ± 1	81 ± 3	>3600	0.72	0.13	0.12	0.03

https://doi.org/10.1021/jacs.6c00684
J. Am. Chem. Soc. 2026, 148, 18903−18918

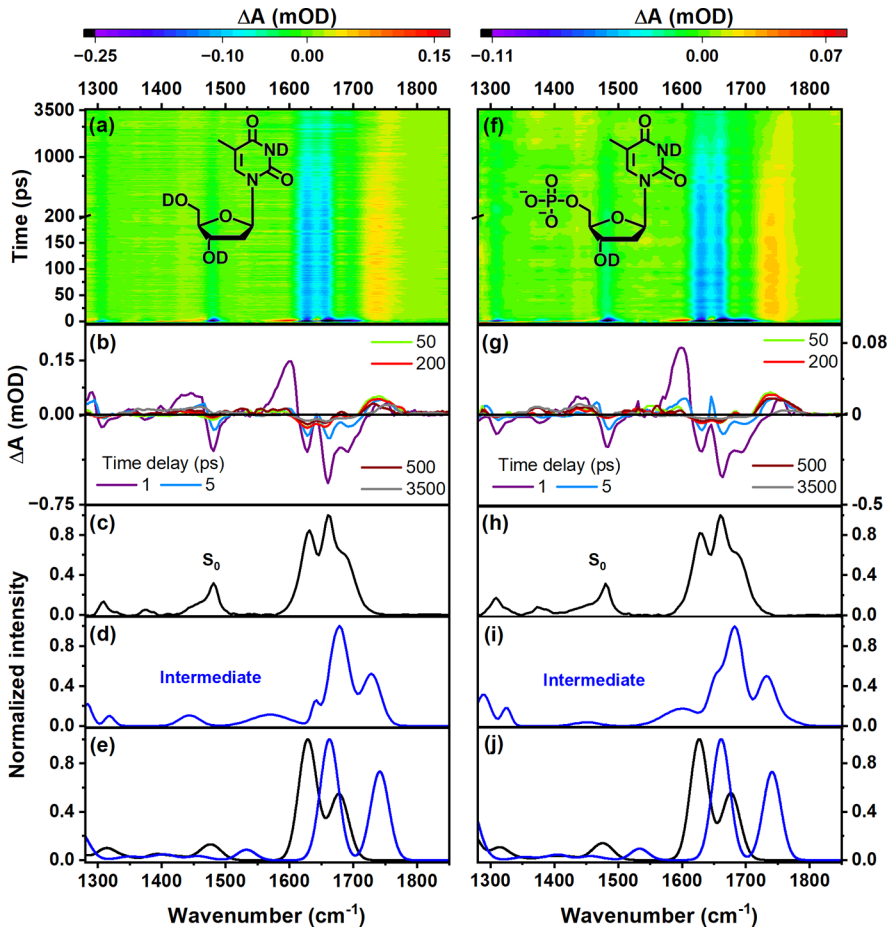

Figure 4. IR-TA spectra measured under 267 nm photoexcitation (a and f), selected lineouts (b and g), static IR spectrum measured for S_0 (c and h), IR spectrum of intermediate species (d and i), and theoretical IR spectra of global minimum (S_0) and twisted intermediate (e and j), for DThd and DTMP in PB-D_2O (20 mM), respectively. In (e) and (j), the theoretical calculations were performed using a harmonic model and DFT at the B3LYP/def2-TZVP+PCM(D_2O) level of theory, assuming the *anti*-rotamer, and considering three explicit D_2O molecules. The calculated frequencies were scaled and stick spectra were convoluted with a Gaussian function, as detailed in Supporting Information Section D(a) and summarized in Table S3.

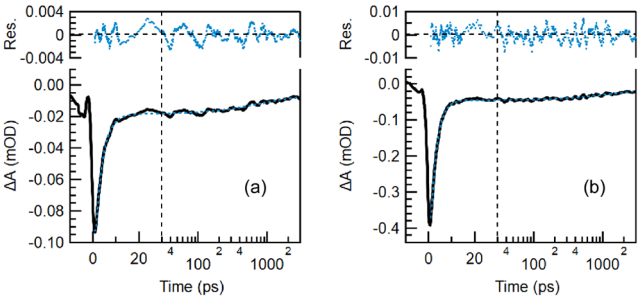

Figure 5. GSBR waveforms (black solid lines) and their exponential fits (blue dashed lines) for (a) DThd (1667 cm^{-1}) and (b) DTMP (1664 cm^{-1}). The waveforms exhibit complex features in the negative time range due to free induction decay in the probe-pump pulse sequence. The horizontal scale is linear up to 30 ps and logarithmic thereafter.

feature of the TIs generated from Cyt derivatives is that they have shorter lifetimes than those for Ura/Thy derivatives, 7.7 ps (reassigning $^1n\pi^*$ to a TI),[18] 43.8 ps,[44] and 51 ps for Cyt, Cyd, and CMP, respectively.

In an EUV-TRPES study of Cyd in aqueous solution by Miura et al.,[27] the decay of the $^1\pi\pi^*$ state excited at 267 nm was analyzed by decomposing the transient signal into four sequential components with lifetimes of 0.07, 0.21, 1.3, and 6 ps. Since the first three components exhibited nearly identical photoelectron spectra, they were attributed to ionization from the same $^1\pi\pi^*$ state, whereas the final 6 ps component was assigned to ionization from the $^1n\pi^*$ state; the QY for the $^1n\pi^*$ state was found to be as low as 0.02. In fluorescence decay measurements of Cyd by Ma et al.,[18] two components with lifetimes of 0.2 and 1.8 ps were identified, whereas a UV-TAS study by Adachi et al.[67] yielded a single lifetime of 0.47 ps. These observations are qualitatively consistent with the aforementioned time constants of 0.07−1.3 ps measured using EUV-TRPES.[27]

The excited-state lifetime of 5-methylcytidine (5m-Cyd) appears to be considerably longer. A pioneering TAS study by Malone et al.[68] reported the lifetime of 5m-Cyd to be 7.2(2) ps. Ma et al. identified two decay components with lifetimes of 0.6 and 5.4 ps.[18] TAS combined with computational simulations by Kabaciński et al.[52] revealed subpicosecond relaxation from the Franck−Condon region to a flat plateau on the $^1\pi\pi^*$ potential-energy surface, followed by population decay from the excited state manifold in 4.3 ps by surmounting a ∼0.35 eV barrier to reach the conical intersection with S_0. The longer lifetime of 5m-Cyd than that of Cyd is consistent with the trend seen for Urd and Thd (or 5-mUrd), and it arises

https://doi.org/10.1021/jacs.6c00684
J. Am. Chem. Soc. 2026, 148, 18903−18918

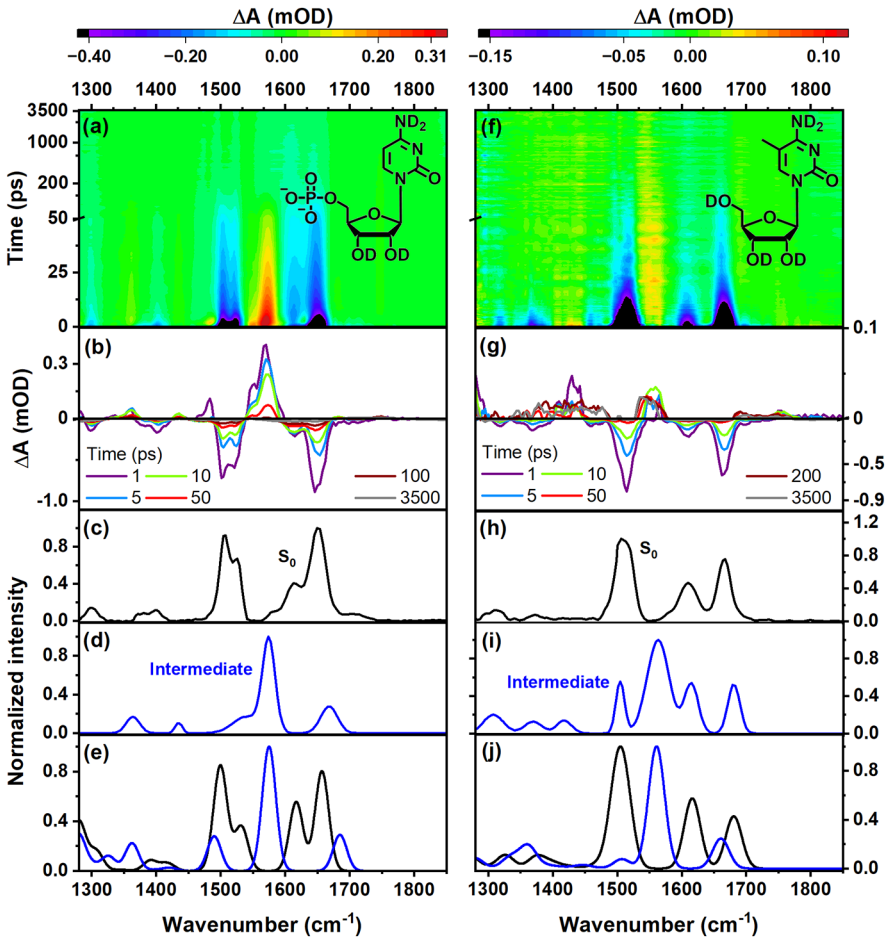

Figure 6. IR-TA spectra measured under 267 nm photoexcitation (a and f), selected lineouts (b and g), static IR spectrum measured for S_0 (c and h), IR spectrum of intermediate species (d and i), and theoretical IR spectra of global minimum (S_0) and twisted intermediate (e and j), for DCMP and 5m-DCyd in PB-D_2O (20 mM), respectively. In (e) and (j), the theoretical calculations were performed using a harmonic model and DFT at the B3LYP/def2-TZVP+PCM(D_2O) level of theory, assuming the *anti*-rotamer, and considering four explicit D_2O molecules. The calculated frequencies were scaled and stick spectra were convoluted with a Gaussian function, as detailed in Supporting Information Section D(a) and summarized in Table S3.

from the presence of a potential barrier to access the conical intersection with S_0 and steric hindrance of the motion of the methyl group caused by the hydration shell. Due to the longer lifetime of the $^1\pi\pi^*$ state, we adapted a slightly different analysis procedure for 5m-DCyd (as described in Supporting Information Section F(e)). Our IR-TAS data and subsequent global fitting (Figures 6f–i and S17) indicate that the $^1\pi\pi^*$ state for 5m-DCyd decays in 8 ps. A blue-shifted C–ND_2 stretching band appears with a rise time of ∼3 ps (Figure S19); it is not clear whether the discrepancy between the $^1\pi\pi^*$ decay time and the rise time for the intermediate is statistically significant. Because the time constants associated with vibrational relaxation and the $^1\pi\pi^*$ state are very similar, they could not be distinguished by GSBR fitting. Consequently, a single-exponential decay model for the twisted intermediate was sufficient to reproduce the GSBR adequately. The results are listed in Table 1, and the GSBR waveforms are shown in Figures S13b and S18. The TI of 5m-Cyd exhibits a very small Φ_{TI} of 0.06 and a τ_{TI}^{eff} of 122 ps. A long-lived triplet state was observed with a low QY (Table 1). The IR absorption spectrum (Figure 6i) of the intermediate agreed reasonably well with the calculated spectrum (Figure 6j).

QM/MM Simulation of Nonadiabatic Dynamics

To clarify the mechanisms of nonadiabatic transitions and TI-forming dynamics, we performed QM/MM surface-hopping dynamical simulations, beginning at the lowest $^1\pi\pi^*$ state, for Urd, Cyd, and Thd in explicit water. As seen in Table 3, these calculations reproduce the experimentally observed trend for Φ_{TI}: Urd exhibits the highest value (0.19), followed by Cyd (0.12) and then Thd (0.05). In all three cases, the nonadiabatic transition to S_0 occurs via the ethylenic conical intersection associated with out-of-plane displacement of the C5=C6 hydrogens (or CH_3 in Thd) and ring puckering.

Figure 7a–c shows the variations of the S_1 and S_0 energies along three representative nuclear trajectories obtained for Urd. Formation of a long-living TI is seen in Figure 7a. In Figure 7b, a TI is only transiently created, whereas direct relaxation to the planar minimum is seen in Figure 7c. Figure 7d shows the nuclear trajectories in the three cases for the two major nuclear displacement coordinates (Q_1, Q_2) involved in the nonadiabatic dynamics: the three trajectories shown in Figure 7a–c are indicated in black, dark green, and light green, respectively. Also indicated as open squares (□) are the Franck–Condon point/planar minimum (FC/$Planar_{min}$) at the bottom left corner, the minimum-energy conical intersection

https://doi.org/10.1021/jacs.6c00684
J. Am. Chem. Soc. 2026, 148, 18903–18918

Table 3. Excited State Lifetime and QY for Twisted Intermediate Formation Extrapolated from QM/MM Molecular Dynamics Simulations at XMS-CASPT2/SA-9-CASSCF(14,10) Level of Theory for Each of the Three Nucleosides, Energy Barrier for Back Reaction toward Planar Global Minimum, and QM/MM Merz−Kollman Charge on C5 and C6 Positions, Computed at RMS-CASPT2/SA-2-CASSCF(6,6) Level of Theory

Sample	Excited state-lifetime (fs)	Φ_{TI}	Energy barrier for back reaction[a] (kcal/mol)	C5/C6 Merz−Kollman charge of twisted intermediate
Urd	138	0.19	3.44 (3.64)	−0.61/0.20
Thd	428	0.05	2.44 (1.69)	−0.22/0.04
Cyd	283	0.12	2.97 (3.31)	−0.57/0.28

[a]These values were obtained optimizing the twisted intermediate and the transition state for the back reaction toward the planar global minimum for uracil, thymine and cytosine in the gas phase. PCM-corrected values to account for water solvent effects are also reported in parentheses. All other columns in this table refer to Urd, Thd and Cyd.

(MECI), and the TI ($Twisted_{min}$) at the bottom right corner. Each of these structures have been fully optimized for all degrees of freedom. The transition state for the back-reaction from the TI to the planar minimum, projected onto this 2D plane, is also indicated as $TS_{projection}$. As seen in the figure, Q_1 is along the displacement direction from $FC/Planar_{min}$ to $Twisted_{min}$, involving torsional/pyramidalization motions without appreciable bond-length changes. Q_2, which is orthogonal to Q_1, corresponds to a displacement from the MECI to its closest point along Q_1, and it primarily involves C5=C6 and N1−C6 bond-length changes (see Figure 8 and Supporting Information Section G(d)). The $TS_{projection}$ lies almost on the bottom axis, with a deviation of only 10°. Because of reflection through the original molecular plane, two symmetry-equivalent regions occur for the multidimensional potential energy surfaces, and the figure depicts one of them. Further details are described in Supporting Information Section G(d). The red and blue colors respectively indicate the regions energetically higher and lower than the MECI.

The nonadiabatic transitions from S_1 to S_0 occur at the positions indicated by filled and open circles, which are distributed in the vicinity of the MECI, where the energy gap between S_1 and S_0 is small. The filled and open circles are associated with the trajectories leading to trapping and nontrapping in the TI, respectively. The open circles are distributed near the MECI, whereas filled circles tend to be closer to the $Twisted_{min}$. Figure 7e displays the nuclear positions and velocities associated with C5 pyramidalization at the nonadiabatic transition (surface hopping) in Urd. The vertical axis corresponds to the degree of pyramidalization (improper C5−C4−C6−H_{C5} torsion), in which the positive and negative regions correspond to two symmetry-equivalent nonplanar conformations; the dynamics in these regions are essentially the same, as mentioned earlier. The results indicate that a nonadiabatic transition occurs at around ±30°. The horizontal axis in Figure 7e depicts the velocity along the C5 pyramidalization coordinate. Notably, when the velocity is oriented in the direction of increasing pyramidalization, the trajectories reach and/or remain in the TI region (Figure 7e). The complete set of QM/MM trajectories is available in Supporting Information Section G(f). Movies of the trajectories are also provided in Supporting Information_2. The results indicate that the nonadiabatic dynamics of Urd are primarily governed by the nuclear momentum along the C5 pyramidalization and hydrogen out-of-plane (HOOP) mode for a nonadiabatic transition; ballistic motion along the reaction coordinate is crucial for TI formation. The importance of HOOP modes as primary key drivers in controlling the outcome of photoinduced ultrafast (≤200 fs) deactivation processes has been already recognized and discussed in the context of retinal systems,[69−72] thus calling for a general controlling mechanism in ultrafast photochemistry.

Figure 7f shows the equivalent (Q_1, Q_2) energy landscape for Thd, which displays considerably longer trapping in the excited state and fewer trajectories reaching the TI. This behavior arises because the hydration shell around the C5 methyl sterically hinders C5=C6 twisting and C5-pyramidalization until it thermally rearranges. Prior to this rearrangement, the initial MECI is considerably higher in energy, making access to the conical intersection energetically prohibitive. The MECI indicated in Figure 7f corresponds to the configuration after solvent rearrangement.

By the time the conical intersection becomes accessible following this rearrangement, vibrational randomization, assisted by intermolecular interactions, reduces the C5 pyramidalization momentum to a much smaller value than in Urd (Figure 7g). As shown in Figures 7g and S28, only two trajectories reach the TI, both with negligible C5 pyramidalization momentum (Figure 7g). The majority of trajectories that lose their pyramidalization momentum experience a ground-state potential force directed toward the planar geometry (Figure S28), which ultimately drives the system back to that configuration (see also Supporting Information Section G(f)).

Thus, the QM/MM study revealed that nucleosides with short excited state lifetimes are in the *dynamical-control* regime; they are driven by a large momentum along the reaction coordinate, achieving a high Φ_{TI}. Urd with the shortest lifetime (Table 3) exhibits the highest Φ_{TI}, followed by Cyd. Thd has an excited state lifetime more than three times longer due to C5 methylation and steric hindrance from the hydration shell.[24] The extended lifetime is associated with vibrational energy randomization, dissipating the momentum initially directed along the reaction coordinate. Consequently, nuclear velocities are much reduced (Figure 7g). This condition is considered to be the *static-control* regime, where the dynamics are dictated by the topography of the potential energy surface at the conical intersection. Consequently, Thd exhibits the lowest Φ_{TI}. As shown in Figure S25, the potential energy landscape from the Franck−Condon region to the conical intersection is similar to Ura and Thy;[24] nevertheless, *dynamical and static control* provide markedly different excited state lifetimes and Φ_{TI} values. As discussed previously,[24] the longer excited state lifetimes of 5-methylated pyrimidines may enable nonadiabatic decay pathways other than that via the ethylenic conical intersection; however, their contributions are less than 10% and cannot account for the reduced Φ_{TI} in Thd.

One point to note here is that previous TAS[24] and EUV-TRPES[73,74] measurements revealed vibrational coherence in the 750 cm^{-1} mode in 5m-Urd and Thd persisting for subpicoseconds. These experimental findings suggest that even though C5 methylation and interactions with the hydration shell promote vibrational energy randomization in modes that are crucial for nonadiabatic dynamics, vibrational coherence is partially preserved in other modes on the subpicosecond time

https://doi.org/10.1021/jacs.6c00684
J. Am. Chem. Soc. 2026, 148, 18903−18918

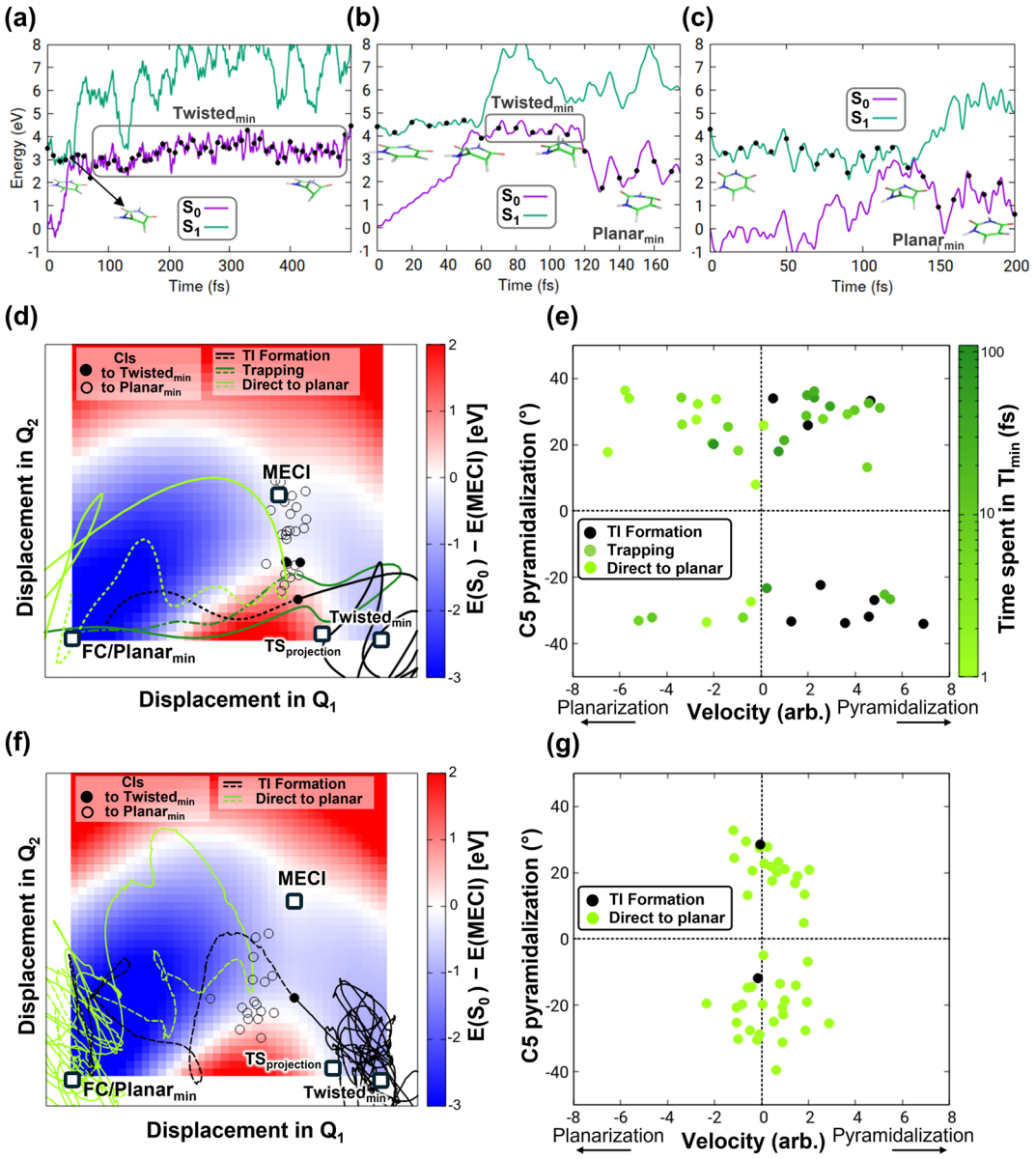

Figure 7. (a–c) Three representative Urd QM/MM trajectories illustrating (a) stable formation of TI, (b) transient trapping in TI region, and (c) direct relaxation to planar global minimum. The populated electronic states are indicated by solid circles. Reactive 2D potential energy surfaces of (d) Urd and (f) Thd (see Supporting Information Section G(f)). Open squares (□) denote the optimized critical geometries (FC/Planar$_{min}$, Twisted$_{min}$, MECI) and the projection of the ground-state transition state for the back reaction (TS$_{projection}$). Hopping points from Urd QM/MM nonadiabatic dynamics are also projected. Solid circles correspond to trajectories forming a stable TI, whereas open circles correspond to trajectories that ultimately return to the planar minimum. The three Urd trajectories shown in (a–c) are projected in (d) as black, dark green, and light green lines, respectively. In (f), two representative Thd trajectories are shown, one leading to the TI and the other returning to the reactant. Dashed and solid lines represent excited and ground-state dynamics, respectively. (e, g) Distribution of velocities along C5 pyramidalization coordinate at hopping points as a function of its instantaneous value (improper torsion C5–C4–C6–H$_{C5}$). Solid black circles correspond to trajectories forming a stable TI, whereas green shading indicates trajectories that populate the TI region only transiently, with darker shading representing longer lifetimes.

scale. In this context, the vibrational randomization discussed here is restricted and is not fully statistical across all vibrational degrees of freedom.

While Φ_{TI} is primarily determined by the topography of the excited state potential energy surface and associated ballistic nuclear motions, τ_{TI}^{eff} (Table 1) is determined by the topography of the ground-state surface. We calculated the planarization energy barrier ($E_{optimized\ transition\text{-}state} - E_{optimized\ twisted\ minimum}$) for gas-phase Ura, Cyt and Thy (Table 3), including implicit solvent (PCM) corrected values (that show the same trend as those computed for the gas phase). The estimated barrier height for Ura and Cyt agree with the relative lifetimes reported for Urd and Cyd (Table 1), while Thy is an outlier showing the lowest barrier (Table 3), at odds with the longest lifetime of the TI observed for Thd (Table 1). It should be noted that the values reported in Table 3 refer to the electronic potential energies and therefore do not correspond to activation free-energy barriers, as entropic contributions are not included. It is noted that motion of the C5 methyl group is more strongly hindered by the solvent than

https://doi.org/10.1021/jacs.6c00684
J. Am. Chem. Soc. 2026, 148, 18903–18918

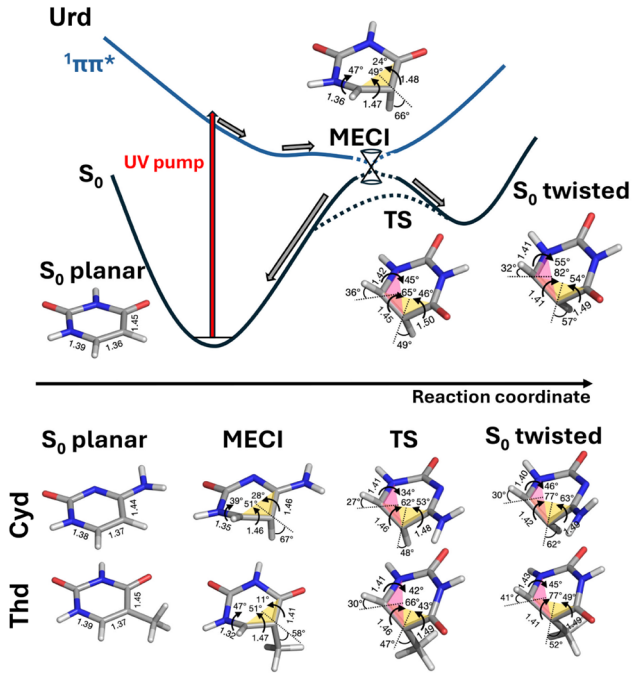

Figure 8. Schematic representation of ground state (S_0) and excited state ($^1\pi\pi^*$) potential energy surfaces showing photoinduced relaxation pathway from planar minimum to minimum-energy conical intersection (MECI) for Urd, followed by decay toward either planar or twisted region of ground state. Analogous energy profiles hold for Cyd and Thd. QM/MM optimized molecular structures at key points along the pathway—planar minimum, MECI, transition state (TS), and twisted minimum—are shown for Urd, Cyd and Thd, together with selected structural parameters (only the structure for the QM region is reported): bond lengths; torsional angles about the C4−C5, C5=C6, and C6−N1 bonds; and out-of-plane bending of the C5 and C6 hydrogens (or methyl group), defined by the C4−C5−C6−H_{C5} (yellow) and C5−C6−N1−H_{C6} (pink) dihedral angles (see Supporting Information Section G(e) and Figure S25).

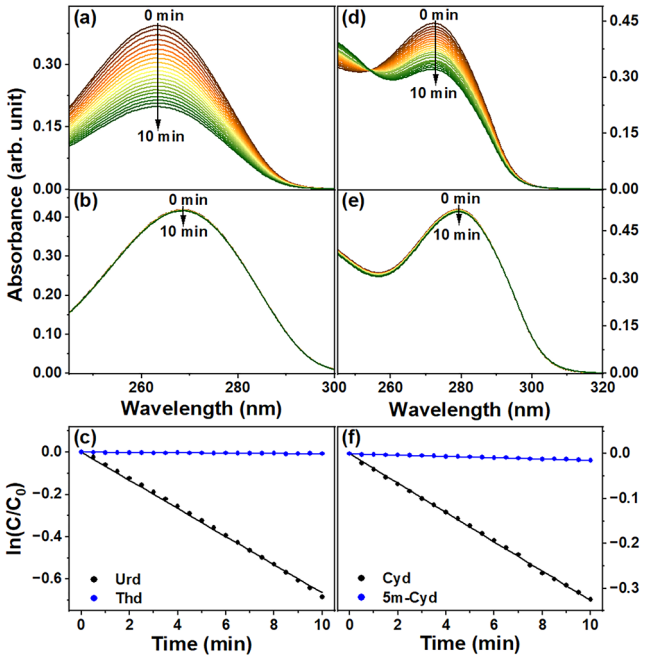

Figure 9. Photoirradiation with 266 nm CW UV laser with incident photon flux of 1.88×10^{18} photons·cm^{-2}·min^{-1}. Change in UV absorption spectra with time for (a) uridine (Urd) and (b) thymidine (Thd), and (c) their photodegradation kinetics. Change in UV absorption spectra with time for (d) cytidine (Cyd) and (e) 5m-Cyd, and (f) their photodegradation kinetics.

that of hydrogen in unmethylated pyrimidines, thus increasing the free-energy barrier with a significant entropic effect (higher mass, slower dynamics, higher solvent displacement). This effectively leads to a higher free-energy barrier than that for Urd and Cyd. Thus, the sole electronic potential energy barrier is not sufficient to explain the behavior of C5-methylated compounds (Figure 8).

Photohydration Measurements

While the hydration reaction rates have been measured extensively in the 1960s,[45] we revisited the measurements for the molecules studied in a comprehensive manner. As an example, Figure 9a,b shows the UV absorption spectra measured as a function of the UV irradiation time for aqueous Urd and Thd, respectively. As described in the Experimental Methods section, the concentrations were adjusted to obtain the same optical densities. Urd exhibits a rapidly decaying absorption intensity, whereas Thd shows only a minor change. A similar difference is seen between Cyd and 5m-Cyd, presented in Figure 9d and e, respectively. These results unambiguously demonstrate a strong influence of C5 methylation on the hydration reaction.

The pseudo-first-order photohydration rate constants (k_{hyd}) obtained for all samples are summarized in Table 4. k_{hyd} for Cyt derivatives have been corrected for the presence of a dehydration (reverse) reaction (see Supporting Information Section E(c)).[6]

DISCUSSION

Nonadiabatic Nuclear Dynamics in Internal Conversion

With some exceptions such as 5m-Cyd, the excited state lifetimes of nucleosides and nucleotides are extremely short. The QM/MM simulations performed in the present study reveal that, particularly in systems such as Urd and Cyd with hydrogen atoms at the C5 and C6 positions, the excited state dynamics involve ballistic trajectories from the Franck−Condon region toward the conical intersection, and further to the TI. When the C5 position is methylated—as in Thd, 5m-Urd or 5m-Cyd—the excited state lifetime is clearly prolonged, and Φ_{TI} decreases. The influence of C5 substitution on the photophysics of these compounds has been repeatedly reported. Malone et al.[68] reported that the lifetimes of the $^1\pi\pi^*$ states of Cyt and Cyd are significantly extended (1 → 7.2 ps) upon C5 substitution. Kabaciński et al.[52] performed sub-30 fs UV-TAS measurements and QM/MM calculations, showing that the $^1\pi\pi^*$ potential-energy surface possesses a barrier between the plateau region and the ethylenic conical intersection, resulting in a longer $^1\pi\pi^*$ lifetime for 5m-Cyd than for Cyd. Ma et al. reported that 5-methylation alters the deactivation pathway,[18] and Martínez-Fernández et al.[23] reported similar results for 5-methyl-2′-deoxycytidine (5m-dCyd). Borrego-Varillas et al.[24] established by QM/MM calculations that the (almost 1 order of magnitude) longer excited state lifetime observed for 5m-Urd with respect to Urd is due to a dynamical barrier along the C5=C6 twisting/pyramidalization mode that emerges in 5m-Urd due to the out-of-plane motion of the C5 methyl that is hindered by water solvent molecules. Wang et al. observed no spectral component

https://doi.org/10.1021/jacs.6c00684
J. Am. Chem. Soc. 2026, 148, 18903−18918

Table 4. QY (Φ_{TI}) and Effective Lifetime (τ_{TI}^{eff}) for Twisted Intermediate and Pseudo-First-Order Photohydration Rate Constant k_{hyd}[a]

Sample	k_{hyd} ($\times 10^{-2}$ min^{-1}) in H_2O	Φ_{TI} in D_2O	τ_{TI}^{eff} in D_2O (ps)[b]	[c]Δq_{TI}^{C6-C5}	$\Phi_{TI} \times \tau_{TI}^{eff}$ (ps)	$k_{hyd}/(\Phi_{TI} \times \tau_{TI}^{eff})$ ($\times 10^7$ s^{-2})
Ura[d]	7.9	0.35	30	0.535	10.5	12.5
Urd	98.6	0.45	334	0.492	150.3	10.9
UMP	86.1	0.50	350	0.463	175	8.2
2′-deoxy-Urd	101.0	0.52	327	0.464	170.0	9.9
5′-deoxy-Urd	98.1	0.49	368	0.538	180.3	9.1
Thy[d]	0.5	0.07	382	0.097	26.8	0.3
Thd	1.2	0.08	813	0.06	65.0	0.3
TMP	0.7	0.05	1177	0.064	58.9	0.2
5m-Urd	1.2	0.11	616	0.036	67.8	0.3
Cyt[e]	14.3[f]	0.25	7.7	0.624	1.9	123.8[f]
Cyd[g]	51.5[f]	0.25	43.8	0.598	11.0	78.4[f]
CMP	75.9[f]	0.22	51	0.535	11.2	112.7[f]
5m-Cyd	2.1	0.06	122	0.09	7.3	4.8

[a]In photoirradiation experiments with incident photon flux of 1.88×10^{18} photons·cm^{-2}·min^{-1}. [b]τ listed here is the value obtained by least-squares fitting assuming a single exponential decay for the twisted intermediate. [c]Calculated from natural population analysis in Gaussian 16 at the B3LYP/def2-TZVP+PCM (H_2O) level of theory. [d]Ref 43. [e]Ref 18, by reassigning $^1n\pi^*$ to twisted intermediate, solvent: H_2O. [f]Corrected considering dehydration rates. [g]Ref 44.

corresponding to a 30 ps lifetime, the hallmark of a TI, for 5m-Cyd under excitation at 240, 266, or 290 nm.[19] QM/MM dynamical simulations revealed that formation of a TI requires ballistic motions involving out-of-plane deformation of the hydrogen atom (or methyl group) attached to the C5=C6 double bond. As the system explores the excited state potential-energy surface, and intramolecular vibrational redistribution occurs, directionality effects in nuclear momentum are lost and trajectories crossing the conical intersection predominantly proceed toward the planar ground-state minimum.

Influence of Molecular Conformation on Nonreactive Relaxation Process

Nucleosides exist as multiple conformers arising from rotation about the glycosidic bond, which interconverts the *syn*- and *anti*-configurations, from ribofuranose puckering between the C3′-endo and C2′-endo forms, and from rotation around the C4′−C5′ bond that modulates the orientation of the 5′-hydroxyl group. These conformations undergo thermal fluctuations and are populated in a statistical ensemble. According to NMR measurements,[58] canonical nucleobases lacking a methyl substituent at the C6 position predominantly adopt the *anti*-conformation about the glycosidic bond in aqueous solution, whereas both ribose puckers are accessible. Interestingly, 5′-deoxy-DUrd without OH at 5′ and DUMP with phosphate at 5′ exhibit dual exponential decay of the TI, suggesting that the orientation of OH at 5′ is unlikely to be the cause of the duality. It is more likely due to 3′-endo and 2′-endo, which are common isomeric forms seen for pyrimidine nucleosides. If the time scale of interconversion among these conformers exceeds the lifetime of the TI, the rate of isomerization of the TI to the planar structure could depend on the specific conformer present. Because the hydration reaction in aqueous solution proceeds slowly, the observed lifetime of the TI is governed primarily by its isomerization to the planar form and thus may encode information associated with the underlying conformational heterogeneity. Indeed, the experimentally observed dual exponential decay for the TI suggests that conformational isomers may influence the decay kinetics. Identifying which structural isomers modulate the rate of planarization, and by what mechanism, involves investigation of subtle intramolecular interactions beyond the scope of the present study and remains a subject for future investigation.

The lifetimes of the TI depend on the molecular structures. Cyt has a far shorter lifetime (<10 ps) than Ura and Thy.[18,44] By binding a ribofuranose group, all of these molecules gain longer TI lifetimes, although Cyd still has the shortest lifetimes among canonical nucleosides.

Hydration Reaction Mediated by Twisted Intermediate

τ_{TI} is limited by isomerization to the planar global minimum in S_0, rather than the photohydration reaction. This is evident from the repeated observations of GSBR in the literature: GSB is almost completely recovered for each photoexcitation cycle. The QY for the hydration reaction has been estimated as 10^{-3}−10^{-2} (see also Table S4).[45]

The molecular systems investigated in this work can be organized into four structurally distinct families: {Ura}, {Thy}, {Cyt}, and {5m-Cyt}. These families differ in two aspects: substitution at the C5 position (hydrogen versus methyl) and the identity of the underlying heterocyclic framework (uracil-type versus cytosine-type). As seen in Table 4 and Figure 10, within the {Ura} family (Ura, Urd, UMP, 2′-deoxyUrd, and 5′-deoxyUrd), a clear correlation can be found between the hydration rate constant k_{hyd} and τ_{TI}^{eff} for the TI. This relationship provides compelling evidence that hydration proceeds through a TI-mediated pathway. While the products are known, the exact mechanistic sequence of elementary steps of photohydration involving the TI remains under investigation. Under neutral conditions, the reaction has been proposed to involve nucleophilic attack of H_2O at C6, as suggested previously by Park et al.[41] The correlation between k_{hyd} and τ_{TI}^{eff} means that the hydration reaction occurs from a thermalized TI after vibrational relaxation. Because Φ_{TI} varies only weakly within this family, the dependence of k_{hyd} on Φ_{TI} does not appear to be very strong; however, k_{hyd} necessarily depends on Φ_{TI}. Thus, the product $\Phi_{TI} \times \tau_{TI}^{eff}$ serves as a physically meaningful descriptor of reactivity, reflecting both population and temporal accessibility of the reactive

https://doi.org/10.1021/jacs.6c00684
J. Am. Chem. Soc. 2026, 148, 18903−18918

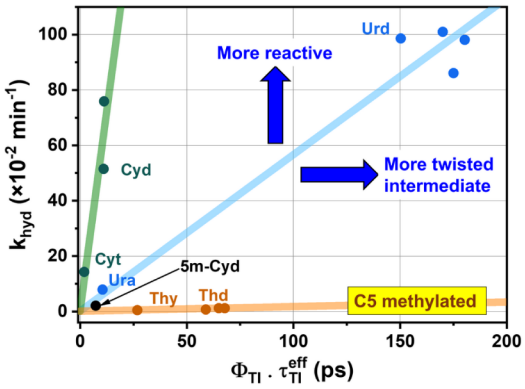

Figure 10. Correlation of photohydration rate with the product of the yield and lifetime of the twisted intermediate, among the same structural family. Blue, green, orange, and black represent {Ura}, {Thy}, {Cyt}, and {5m-Cyt} families, respectively.

configuration. This interpretation is fully consistent with the kinetic model discussed in Supporting Information Section F(g). Please note that, in this analysis, k_{hyd} was measured in H_2O rather than D_2O, which would ideally be required for direct comparison with Φ_{TI} and τ_{TI}. Because the kinetic isotope effect on the hydration reaction is expected to be very similar across the molecular series examined, our conclusion on the distinct dependence of $k_{hyd}/(\Phi_{TI} \times \tau_{TI}^{eff})$ on molecular structure remains unaffected.

A quantitatively different reactivity is observed for the {Thy} family (Thy, Thd, TMP, and 5m-Urd), which systematically exhibits lower hydration rates relative to the {Ura} family. The diminished reactivity cannot be rationalized in terms of the TI population, as seen by low values of the normalized index $k_{hyd}/(\Phi_{TI} \times \tau_{TI}^{eff})$. The origin lies in intrinsic electronic properties of the TI for {Thy}. As established in the studies in the 1960s, the hydration reaction proceeds via preferential insertion of OH at the C6 position, which is attributed to a partial positive charge on C6.[41,45] The C5 methylation reduces the electric polarization of the C5=C6 bond (Δq_{TI}^{C6-C5}), attenuating its susceptibility to attack by solvent water. Thus, the C5 methylation influences k_{hyd} not only through Φ_{TI} but also through the intrinsic reactivity of the TI.

An analogous substituent-dependent modulation is observed in the Cyt series when comparing {Cyt} with 5m-Cyd, further supporting the conclusion that C5 substitution directly influences the electronic polarization governing hydration. At the same time, a clear separation in $k_{hyd}/(\Phi_{TI} \times \tau_{TI}^{eff})$ between uracil-type and cytosine-type frameworks indicates that the intrinsic heterocyclic framework exerts an additional and independent influence.

As for the nature of the twisted C5=C6 bond, electronic structure calculations reveal that for each pyrimidine nucleoside the TI is not a zwitterionic species as highlighted by a Merz–Kollman molecular-charge analysis on C5 and C6 positions (Table 3). It also does not display a pure diradical character, since the occupation numbers for the frontier natural orbitals are close to 2 and 0 (1.78 and 0.22, respectively: see Figure S30), thus pointing more to a closed-shell system in agreement with previous studies on gas-phase nucleobases by Park et al.[41] and Obara et al.[43] The strong twisting around the C5=C6 double bond experienced by the TI (83° in Urd, 77° in Cyd and Thd) results in an elongation, and thus a weakening, of this bond with respect to the planar global minimum (from 1.36 Å to 1.41 Å in Urd, 1.37 Å to 1.42 Å in Cyd and 1.37 Å to 1.41 Å in Thd) (Figure 8). This is accompanied by localization of the electron density on C5 and C6 atoms, as evidenced by the shape of frontier natural orbitals (Figure S30). Assuming that the hydration reaction is initiated by the nucleophilic attack of water oxygen at the C6 position, a higher positive charge on this atom would favor this reaction. A Merz–Kollman charge analysis of the three nucleosides (Table 3) and a natural population analysis of all molecules (Table 4) reflects the experimental intrinsic reactivity index (Table 4) with Urd showing the largest positive charge on C6, followed by Cyd and Thd, which further supports the hypothesis that methylation at C5 not only reduces Φ_{TI} but also suppresses the reactivity.

Due to a rather small barrier for ground-state isomerization back to the global minimum (Table 3), the TI is not highly reactive with respect to hydration (Table S4). Recently, Mathew et al.[75] reported the solvent isotope effect on the lifetime of the TI generated from Ura and attributed it to a hydration reaction. However, the QY for the hydration reaction is far too low[45] (see also Table S4) to influence the lifetime of the TI, as evidenced by the GSBR results reported so far. Thus, the solvent isotope effect they measured is likely due to a planarization process.

Taken together, these results demonstrate that TI-mediated hydration is governed by an interplay between nonadiabatic population dynamics and intrinsic electronic reactivity. While excited state dynamics determine access to and (in part) residence within the TI, the ultimate hydration efficiency is dictated by how the molecular framework and C5 substitution shape the charge redistribution along the reactive C5=C6 bond.

CONCLUSIONS

In conclusion, we have elucidated the formation, decay, and reactivity of a ground-state TI that governs the ultrafast internal conversion and subsequent photohydration of UV-excited pyrimidine nucleosides and nucleotides in aqueous solution. Infrared transient absorption spectroscopy unambiguously identifies a TI characterized by a strongly twisted C5=C6 double bond, and its quantum yield (Φ_{TI}) and lifetime (τ_{TI}^{eff}) are shown to depend sensitively on molecular structure.

A clear correlation between $\Phi_{TI} \times \tau_{TI}^{eff}$ and the photohydration rate constant (k_{hyd}) demonstrates that the TI mediates hydration damage. Comparison of C5–H and C5-methylated species reveals pronounced differences in both Φ_{TI} and $k_{hyd}/(\Phi_{TI} \times \tau_{TI}^{eff})$, establishing C5 methylation as a critical modulator of photochemistry for these compounds. Our QM/MM dynamical simulations show that TI formation requires sufficient nuclear momentum along the reaction coordinate at the conical intersection, and that C5 methylation suppresses both this momentum and Φ_{TI}. Importantly, even after accounting for the reduced Φ_{TI}, the reactivity index $k_{hyd}/(\Phi_{TI} \times \tau_{TI}^{eff})$ ratio remains significantly lower for C5-methylated compounds, indicating an intrinsic decrease in the chemical reactivity of the TI itself. The TI is neither diradical nor zwitterionic in character but instead features an elongated and polarized C5=C6 double bond, whose polarization and hydration reactivity are attenuated by C5 methylation.

https://doi.org/10.1021/jacs.6c00684
J. Am. Chem. Soc. 2026, 148, 18903–18918

A vibrationally hot TI rapidly relaxes in the basin corresponding to the TI and then returns to the planar ground-state minimum in most cases. A high activation barrier limits the overall photohydration QY to a low value (~0.01). In addition, τ_{TI}^{eff}, which is inversely proportional to the planarization rate, exhibits a dual structural dependence, most likely reflecting the influence of different ribose puckering configurations. To elucidate this issue, we plan to conduct analogous experiments using bridged locked nucleic acids (LNAs), in which the ribose ring is conformationally locked and cannot undergo puckering.

The present study establishes a unified mechanistic framework connecting nonadiabatic electronic relaxation, twisting dynamics, and chemical reactivity, and demonstrates how C5 methylation—most prominently in thymidine—enhances photostability by suppressing both the formation and intrinsic reactivity of a key ground-state intermediate. The same mechanism accounts for the reduced photohydration of 5m-Cyd relevant to epigenetics. However, when these molecules are incorporated into stranded nucleic acid structures, they are subject to an alternative photodamage pathway, cyclobutane pyrimidine dimer formation, leading to relative photostabilities that differ from those of the monomers. The details will be discussed elsewhere.

■ ASSOCIATED CONTENT

Data Availability Statement

The data presented here are available upon request at suzuki@kuchem.kyoto-u.ac.jp.

Supporting Information

The Supporting Information is available free of charge at https://pubs.acs.org/doi/10.1021/jacs.6c00684.

Photoexcitation conditions; chemicals; proton NMR; simulation of IR spectra; IR spectra simulated using explicit solvent molecules; calculations for *syn*- and *anti*-rotamers; photodegradation experiment setup; calculation of true photohydration rate and photohydration quantum yield; reversibility of photodegradation; additional photodegradation studies; isotopic effect on photodegradation; effect of sugar moiety on photodegradation; kinetic analysis of hydration reaction; IR-TAS of additional nucleosides; ground state bleach recovery (GSBR); vibrational frequency dependence of GSBR and positive marker-band dynamics; feasibility of differentiating isomers of twisted intermediate; detailed analysis for 5m-DCyd; QM/MM setup; active spaces for dynamics and RMS-CASPT2; construction of reactive PES; additional dynamical information; QM/MM molecular dynamic simulations for Urd, Thd and Cyd; frontier natural orbitals of the twisted intermediate of solvated uridine; calculation of the charge on C5 and C6 (PDF)

Optimized geometries and movies of the Urd and Thd trajectories projected onto the reactive 2D potential energy surface (ZIP)

■ AUTHOR INFORMATION

Corresponding Authors

Toshinori Suzuki − *Department of Chemistry, Graduate School of Science, Kyoto University, Kyoto 606-8502, Japan;* orcid.org/0000-0002-4603-9168; Email: suzuki@kuchem.kyoto-u.ac.jp

Marco Garavelli − *Dipartimento di Chimica industriale "Toso Montanari", Università di Bologna, Bologna 40129, Italy;* orcid.org/0000-0002-0796-289X; Email: marco.garavelli@unibo.it

Irene Conti − *Dipartimento di Chimica industriale "Toso Montanari", Università di Bologna, Bologna 40129, Italy;* orcid.org/0000-0001-7982-4480; Email: irene.conti@unibo.it

Authors

Srijon Ghosh − *Department of Chemistry, Graduate School of Science, Kyoto University, Kyoto 606-8502, Japan;* orcid.org/0000-0002-2056-2532

Yuki Obara − *Department of Chemistry, Graduate School of Science, Kyoto University, Kyoto 606-8502, Japan;* orcid.org/0000-0003-2206-9618

Vishal Kumar Jaiswal − *Dipartimento di Chimica industriale "Toso Montanari", Università di Bologna, Bologna 40129, Italy;* orcid.org/0000-0002-5090-7984

Mario Taddei − *Dipartimento di Chimica industriale "Toso Montanari", Università di Bologna, Bologna 40129, Italy*

Artur Nenov − *Dipartimento di Chimica industriale "Toso Montanari", Università di Bologna, Bologna 40129, Italy;* orcid.org/0000-0003-3071-5341

Complete contact information is available at: https://pubs.acs.org/10.1021/jacs.6c00684

Author Contributions

#S.G., Y.O., V.K.J., and M.T. contributed equally.

Notes

The authors declare no competing financial interest.

■ ACKNOWLEDGMENTS

This work was supported by the Japan Society for the Promotion of Science (JSPS) KAKENHI Grant (No. 21H04970). S.G. appreciates JSPS for the postdoctoral fellowship. Computation time was provided by the supercomputer systems of both the Institute for Chemical Research and the Academic Center for Computing and Media Studies, Kyoto University. We would like to thank Dr. Saki Maejima for NMR measurements and Takuya Mae for his assistance with photodegradation measurements.

■ REFERENCES

(1) Watson, J. D.; Crick, F. H. C. Molecular Structure of Nucleic Acids: A Structure for Deoxyribose Nucleic Acid. *Nature* **1953**, *171* (4356), 737−738.

(2) Barbatti, M.; Aquino, A. J. A.; Szymczak, J. J.; Nachtigallová, D.; Hobza, P.; Lischka, H. Relaxation mechanisms of UV-photoexcited DNA and RNA nucleobases. *Proc. Natl. Acad. Sci. U. S. A.* **2010**, *107* (50), 21453−21458.

(3) Crespo-Hernández, C. E.; Cohen, B.; Hare, P. M.; Kohler, B. Ultrafast Excited-State Dynamics in Nucleic Acids. *Chem. Rev.* **2004**, *104* (4), 1977−2020.

(4) Improta, R.; Santoro, F.; Blancafort, L. Quantum Mechanical Studies on the Photophysics and the Photochemistry of Nucleic Acids and Nucleobases. *Chem. Rev.* **2016**, *116* (6), 3540−3593.

(5) Markovitsi, D. UV-induced DNA Damage: The Role of Electronic Excited States. *Photochem. Photobiol.* **2016**, *92* (1), 45−51.

(6) Eisinger, J.; Shulman, R. G. Excited Electronic States of DNA. *Science* **1968**, *161* (3848), 1311−1319.

(7) Setlow, R. B. Cyclobutane-Type Pyrimidine Dimers in Polynucleotides. *Science* **1966**, *153* (3734), 379−386.
(8) Schreier, W. J.; Schrader, T. E.; Koller, F. O.; Gilch, P.; Crespo-Hernández, C. E.; Swaminathan, V. N.; Carell, T.; Zinth, W.; Kohler, B. Thymine Dimerization in DNA Is an Ultrafast Photoreaction. *Science* **2007**, *315* (5812), 625−629.
(9) McKenzie, R. L.; Aucamp, P. J.; Bais, A. F.; Björn, L. O.; Ilyas, M.; Madronich, S. Ozone depletion and climate change: Impacts on UV radiation. *Photochem. Photobiol. Sci.* **2011**, *10* (2), 182−198.
(10) Liu, J.; Hardisty, D. S.; Kasting, J. F.; Fakhraee, M.; Planavsky, N. J. Evolution of the iodine cycle and the late stabilization of the Earth's ozone layer. *Proc. Natl. Acad. Sci. U. S. A.* **2025**, *122* (2), No. e2412898121.
(11) Merchán, M.; Serrano-Andrés, L. Ultrafast Internal Conversion of Excited Cytosine via the Lowest $\pi\pi^*$ Electronic Singlet State. *J. Am. Chem. Soc.* **2003**, *125* (27), 8108−8109.
(12) Matsika, S. Radiationless Decay of Excited States of Uracil through Conical Intersections. *J. Phys. Chem. A* **2004**, *108* (37), 7584−7590.
(13) Perun, S.; Sobolewski, A. L.; Domcke, W. Conical Intersections in Thymine. *J. Phys. Chem. A* **2006**, *110* (49), 13238−13244.
(14) Hare, P. M.; Crespo-Hernández, C. E.; Kohler, B. Internal conversion to the electronic ground state occurs via two distinct pathways for pyrimidine bases in aqueous solution. *Proc. Natl. Acad. Sci. U. S. A.* **2007**, *104* (2), 435−440.
(15) Stange, U. C.; Temps, F. Ultrafast electronic deactivation of UV-excited adenine and its ribo- and deoxyribonucleosides and -nucleotides: A comparative study. *Chem. Phys.* **2018**, *515*, 441−451.
(16) Gustavsson, T.; Bányász, Á.; Lazzarotto, E.; Markovitsi, D.; Scalmani, G.; Frisch, M. J.; Barone, V.; Improta, R. Singlet excited-state behavior of uracil and thymine in aqueous solution: A combined experimental and computational study of 11 uracil derivatives. *J. Am. Chem. Soc.* **2006**, *128* (2), 607−619.
(17) Pilles, B. M.; Maerz, B.; Chen, J.; Bucher, D. B.; Gilch, P.; Kohler, B.; Zinth, W.; Fingerhut, B. P.; Schreier, W. J. Decay pathways of thymine revisited. *J. Phys. Chem. A* **2018**, *122* (21), 4819−4828.
(18) Ma, C.; Cheng, C. C.-W.; Chan, C. T.-L.; Chan, R. C.-T.; Kwok, W.-M. Remarkable effects of solvent and substitution on the photo-dynamics of cytosine: A femtosecond broadband time-resolved fluorescence and transient absorption study. *Phys. Chem. Chem. Phys.* **2015**, *17* (29), 19045−19057.
(19) Wang, X.; Zhou, Z.; Tang, Y.; Chen, J.; Zhong, D.; Xu, J. Excited state decay pathways of 2′-deoxy-5-methylcytidine and deoxycytidine revisited in solution: A comprehensive kinetic study by femtosecond transient absorption. *J. Phys. Chem. B* **2018**, *122* (28), 7027−7037.
(20) Xue, B.; Yabushita, A.; Kobayashi, T. Ultrafast dynamics of uracil and thymine studied using a sub-10 fs deep ultraviolet laser. *Phys. Chem. Chem. Phys.* **2016**, *18* (25), 17044−17053.
(21) Prokhorenko, V. I.; Picchiotti, A.; Pola, M.; Dijkstra, A. G.; Miller, R. D. New insights into the photophysics of DNA nucleobases. *J. Phys. Chem. Lett.* **2016**, *7* (22), 4445−4450.
(22) Hua, X.; Hua, L.; Liu, X. The methyl-and aza-substituent effects on nonradiative decay mechanisms of uracil in water: A transient absorption study in the UV region. *Phys. Chem. Chem. Phys.* **2016**, *18* (20), 13904−13911.
(23) Martínez-Fernández, L.; Pepino, A.; Segarra-Martí, J.; Jovaisaite, J.; Vaya, I.; Nenov, A.; Markovitsi, D.; Gustavsson, T.; Banyasz, A.; Garavelli, M.; et al. Photophysics of deoxycytidine and 5-methyldeoxycytidine in solution: A comprehensive picture by quantum mechanical calculations and femtosecond fluorescence spectroscopy. *J. Am. Chem. Soc.* **2017**, *139* (23), 7780−7791.
(24) Borrego-Varillas, R.; Nenov, A.; Kabaciński, P.; Conti, I.; Ganzer, L.; Oriana, A.; Jaiswal, V. K.; Delfino, I.; Weingart, O.; Manzoni, C.; et al. Tracking excited state decay mechanisms of pyrimidine nucleosides in real time. *Nat. Commun.* **2021**, *12* (1), 7285.
(25) Buchner, F.; Nakayama, A.; Yamazaki, S.; Ritze, H.-H.; Lübcke, A. Excited-state relaxation of hydrated thymine and thymidine measured by liquid-jet photoelectron spectroscopy: Experiment and simulation. *J. Am. Chem. Soc.* **2015**, *137* (8), 2931−2938.
(26) Erickson, B. A.; Heim, Z. N.; Pieri, E.; Liu, E.; Martinez, T. J.; Neumark, D. M. Relaxation dynamics of hydrated thymine, thymidine, and thymidine monophosphate probed by liquid jet time-resolved photoelectron spectroscopy. *J. Phys. Chem. A* **2019**, *123* (50), 10676−10684.
(27) Miura, Y.; Yamamoto, Y.-I.; Karashima, S.; Orimo, N.; Hara, A.; Fukuoka, K.; Ishiyama, T.; Suzuki, T. Formation of long-lived dark states during electronic relaxation of pyrimidine nucleobases studied using extreme ultraviolet time-resolved photoelectron spectroscopy. *J. Am. Chem. Soc.* **2023**, *145* (6), 3369−3381.
(28) Orimo, N.; Yamamoto, Y.-I.; Karashima, S.; Boyer, A.; Suzuki, T. Ultrafast electronic relaxation in 6-methyluracil and 5-fluorouracil in isolated and aqueous conditions: Substituent and solvent effects. *J. Phys. Chem. Lett.* **2023**, *14* (11), 2758−2763.
(29) Ullrich, S.; Schultz, T.; Zgierski, M. Z.; Stolow, A. Electronic relaxation dynamics in DNA and RNA bases studied by time-resolved photoelectron spectroscopy. *Phys. Chem. Chem. Phys.* **2004**, *6* (10), 2796−2801.
(30) Wolf, T. J.; Parrish, R. M.; Myhre, R. H.; Martínez, T. J.; Koch, H.; Gühr, M. Observation of ultrafast intersystem crossing in thymine by extreme ultraviolet time-resolved photoelectron spectroscopy. *J. Phys. Chem. A* **2019**, *123* (32), 6897−6903.
(31) Merchán, M.; Serrano-Andrés, L.; Robb, M. A.; Blancafort, L. Triplet-state formation along the ultrafast decay of excited singlet cytosine. *J. Am. Chem. Soc.* **2005**, *127* (6), 1820−1825.
(32) Nachtigallová, D.; Aquino, A. J.; Szymczak, J. J.; Barbatti, M.; Hobza, P.; Lischka, H. Nonadiabatic dynamics of uracil: Population split among different decay mechanisms. *J. Phys. Chem. A* **2011**, *115* (21), 5247−5255.
(33) Boldissar, S.; de Vries, M. S. How nature covers its bases. *Phys. Chem. Chem. Phys.* **2018**, *20* (15), 9701−9716.
(34) Arpa, E. M.; Brister, M. M.; Hoehn, S. J.; Crespo-Hernández, C. E.; Corral, I. On the origin of the photostability of DNA and RNA monomers: Excited state relaxation mechanism of the pyrimidine chromophore. *J. Phys. Chem. Lett.* **2020**, *11* (13), 5156−5161.
(35) Milovanović, B.; Novak, J.; Etinski, M.; Domcke, W.; Došlić, N. Simulation of UV absorption spectra and relaxation dynamics of uracil and uracil−water clusters. *Phys. Chem. Chem. Phys.* **2021**, *23* (4), 2594−2604.
(36) Szabla, R.; Kruse, H.; Šponer, J.; Góra, R. W. Water−chromophore electron transfer determines the photochemistry of cytosine and cytidine. *Phys. Chem. Chem. Phys.* **2017**, *19* (27), 17531−17537.
(37) De Camillis, S.; Miles, J.; Alexander, G.; Ghafur, O.; Williams, I. D.; Townsend, D.; Greenwood, J. B. Ultrafast non-radiative decay of gas-phase nucleosides. *Phys. Chem. Chem. Phys.* **2015**, *17* (36), 23643−23650.
(38) Pepino, A. J.; Segarra-Martí, J.; Nenov, A.; Rivalta, I.; Improta, R.; Garavelli, M. UV-induced long-lived decays in solvated pyrimidine nucleosides resolved at the MS-CASPT2/MM level. *Phys. Chem. Chem. Phys.* **2018**, *20* (10), 6877−6890.
(39) Chakraborty, P.; Liu, Y.; McClung, S.; Weinacht, T.; Matsika, S. Time resolved photoelectron spectroscopy as a test of electronic structure and nonadiabatic dynamics. *J. Phys. Chem. Lett.* **2021**, *12* (21), 5099−5104.
(40) Park, W.; Lee, S.; Huix-Rotllant, M.; Filatov, M.; Choi, C. H. Impact of the dynamic electron correlation on the unusually long excited-state lifetime of thymine. *J. Phys. Chem. Lett.* **2021**, *12* (18), 4339−4346.
(41) Park, W.; Filatov, M.; Sadiq, S.; Gerasimov, I.; Lee, S.; Joo, T.; Choi, C. H. A Plausible Mechanism of Uracil Photohydration Involves an Unusual Intermediate. *J. Phys. Chem. Lett.* **2022**, *13* (30), 7072−7080.
(42) Yu, H.; Sanchez-Rodriguez, J. A.; Pollum, M.; Crespo-Hernández, C. E.; Mai, S.; Marquetand, P.; González, L.; Ullrich, S. Internal conversion and intersystem crossing pathways in UV excited,

isolated uracils and their implications in prebiotic chemistry. *Phys. Chem. Chem. Phys.* **2016**, *18* (30), 20168−20176.
(43) Obara, Y.; Ghosh, S.; Humeniuk, A.; Kamibashira, S.; Adachi, S.; Suzuki, T. Formation of Ground-State Intermediate during Electronic Relaxation of Pyrimidine Nucleobases. *J. Am. Chem. Soc.* **2025**, *147* (18), 15077−15087.
(44) Obara, Y.; Ghosh, S.; Kamibashira, S.; Suzuki, T. Solvent Effects on the Formation of Ground-State Twisted Intermediate during Electronic Relaxation of Pyrimidine Nucleobases. *J. Am. Chem. Soc.* **2025**, *147* (45), 41284−41296.
(45) Fisher, G. J.; Johns, H. E. 4 - Pyrimidine Photohydrates. In *Photochemistry and Photobiology of Nucleic Acids*. Wang, S. Y., ed.; Academic Press, 1976; pp 169−224.
(46) Brown, I. H.; Johns, H. E. Photochemistry of Uracil. Intersystem Crossing and Dimerization in Aqueous Solution. *Photochem. Photobiol.* **1968**, *8* (4), 273−286.
(47) Wechter, W. J.; Smith, K. C. Structure and chemistry of uridine photohydrate. *Biochemistry* **1968**, *7* (11), 4064−4069.
(48) Liu, F.-T.; Yang, N. C. Photochemistry of cytosine derivatives. 2. Photohydration of cytosine derivatives. Proton magnetic resonance study on the chemical structure and property of photohydrates. *Biochemistry* **1978**, *17* (23), 4877−4885.
(49) Wang, S. Y.; Nnadi, J. C. Mechanism for the photohydration of pyrimidines. *Chem. Commun.* **1968**, *19*, 1160−1162.
(50) Burr, J. G.; Gordon, B. R.; Park, E. H. The mechanism of photohydration of uracil and N-substituted uracils. *Photochem. Photobiol.* **1968**, *8* (1), 73−78.
(51) Chakraborty, P.; Karsili, T. N. V.; Marchetti, B.; Matsika, S. Mechanistic insights into photoinduced damage of DNA and RNA nucleobases in the gas phase and in bulk solution. *Faraday Discuss* **2018**, *207*, 329−350.
(52) Kabaciński, P.; Romanelli, M.; Ponkkonen, E.; Jaiswal, V. K.; Carell, T.; Garavelli, M.; Cerullo, G.; Conti, I. Unified Description of Ultrafast Excited State Decay Processes in Epigenetic Deoxycytidine Derivatives. *J. Phys. Chem. Lett.* **2021**, *12* (45), 11070−11077.
(53) Snellenburg, J. J.; Laptenok, S.; Seger, R.; Mullen, K. M.; van Stokkum, I. H. M. Glotaran: A Java-Based Graphical User Interface for the R Package TIMP. *J. Stat. Soft* **2012**, *49* (3), 1−22.
(54) Becke, A. D. Density-Functional Thermochemistry. III. The Role of Exact Exchange. *J. Chem. Phys.* **1993**, *98* (7), 5648−5652.
(55) Weigend, F.; Ahlrichs, R. Balanced Basis Sets of Split Valence, Triple Zeta Valence And Quadruple Zeta Valence Quality for H To Rn: Design And Assessment of Accuracy. *Phys. Chem. Chem. Phys.* **2005**, *7* (18), 3297−3305.
(56) Frisch, M. J.; Trucks, G. W.; Schlegel, H. B.; Scuseria, G. E.; Robb, M. A.; Cheeseman, J. R.; Scalmani, G.; Barone, V.; Petersson, G. A.; Nakatsuji, H., et al. *Gaussian 16 Rev. C.01*; Gaussian, Inc.: Wallingford, CT, 2016.
(57) Martinez-Fernandez, L.; Improta, R. The photophysics of protonated cytidine and hemiprotonated cytidine base pair: A computational study. *Photochem. Photobiol.* **2024**, *100* (2), 314−322.
(58) Schweizer, M. P.; Banta, E. B.; Witkowski, J. T.; Robins, R. K. Determination of pyrimidine nucleoside syn-anti conformational preference in solution by proton and carbon-13 nuclear magnetic resonance. *J. Am. Chem. Soc.* **1973**, *95* (11), 3770−3778.
(59) Hammes-Schiffer, S.; Tully, J. C. Proton transfer in solution: Molecular dynamics with quantum transitions. *J. Chem. Phys.* **1994**, *101* (6), 4657−4667.
(60) Tully, J. C. Molecular dynamics with electronic transitions. *J. Chem. Phys.* **1990**, *93* (2), 1061−1071.
(61) Weingart, O.; Nenov, A.; Altoè, P.; Rivalta, I.; Segarra-Martí, J.; Dokukina, I.; Garavelli, M. COBRAMM 2.0 —— A software interface for tailoring molecular electronic structure calculations and running nanoscale (QM/MM) simulations. *J. Mol. Model* **2018**, *24* (9), 271.
(62) Li Manni, G.; Fdez Galván, I.; Alavi, A.; Aleotti, F.; Aquilante, F.; Autschbach, J.; Avagliano, D.; Baiardi, A.; Bao, J. J.; Battaglia, S.; et al. The OpenMolcas Web: A Community-Driven Approach to Advancing Computational Chemistry. *J. Chem. Theory Comput.* **2023**, *19* (20), 6933−6991.
(63) Case, D. A.; Aktulga, H. M.; Belfon, K.; Ben-Shalom, I. Y.; Berryman, J. T.; Brozell, S. R.; Carvahol, F. S.; Cerutti, D. S.; Cheatham, T. E., III; Cisneros, G. A., et al. *AMBER 2025*; University of California: San Francisco, 2025.
(64) Lu, T.; Chen, F. Multiwfn: A multifunctional wavefunction analyzer. *J. Comput. Chem.* **2012**, *33* (5), 580−592.
(65) Zhang, J. LIBERTA: Computerized optimization and code synthesis for electron repulsion integral evaluation. *J. Chem. Theory Comput.* **2018**, *14* (2), 572−587.
(66) Brister, M. M.; Crespo-Hernández, C. E. Excited-State Dynamics in the RNA Nucleotide Uridine 5′-Monophosphate Investigated Using Femtosecond Broadband Transient Absorption Spectroscopy. *J. Phys. Chem. Lett.* **2019**, *10* (9), 2156−2161.
(67) Adachi, S.; Obara, Y.; Shiomoto, R.; Suzuki, T. Influence of C5 Methylation on Cytidine Photohydration Revealed by Deep-Ultraviolet Transient Absorption Anisotropy Spectroscopy. *J. Phys. Chem. Lett.* **2025**, *16* (45), 11717−11723.
(68) Malone, R. J.; Miller, A. M.; Kohler, B. Singlet Excited-state Lifetimes of Cytosine Derivatives Measured by Femtosecond Transient Absorption. *Photochem. Photobiol.* **2003**, *77* (2), 158−164.
(69) Kukura, P.; McCamant, D. W.; Yoon, S.; Wandschneider, D. B.; Mathies, R. A. Structural Observation of the Primary Isomerization in Vision with Femtosecond-Stimulated Raman. *Science* **2005**, *310* (5750), 1006−1009.
(70) Weingart, O. The role of HOOP-modes in the ultrafast photoisomerization of retinal models. *Chem. Phys.* **2008**, *349* (1), 348−355.
(71) Weingart, O.; Altoè, P.; Stenta, M.; Bottoni, A.; Orlandi, G.; Garavelli, M. Product formation in rhodopsin by fast hydrogen motions. *Phys. Chem. Chem. Phys.* **2011**, *13* (9), 3645−3648.
(72) Polli, D.; Altoè, P.; Weingart, O.; Spillane, K. M.; Manzoni, C.; Brida, D.; Tomasello, G.; Orlandi, G.; Kukura, P.; Mathies, R. A.; et al. Conical intersection dynamics of the primary photoisomerization event in vision. *Nature* **2010**, *467* (7314), 440−443.
(73) Karashima, S.; Suzuki, T. Exploring the Vibrational Coherences in the Ultrafast Electronic Relaxation of Pyrimidine Nucleobases and Nucleosides. *J. Am. Chem. Soc.* **2025**, *147* (3), 2291−2295.
(74) Karashima, S.; Suzuki, T. Evidence for a Twisted Intermediate in Gaseous Uracil Revealed by Photoelectron Quantum Beats. *J. Phys. Chem. Lett.* **2025**, *16* (46), 12045−12049.
(75) Mathew, R.; Tonny, T. I.; Crespo-Hernández, C. E. UV Excitation of Uracil Results in the Formation of a Ground-State Intermediate in Less Than One Picosecond and Its Decay is Quenched by Nucleophilic Water Addition. *J. Am. Chem. Soc.* **2025**, *147* (45), 41237−41241.

NOTE ADDED AFTER ASAP PUBLICATION

A methyl group was added to the molecular structure in Figure 4a on May 13, 2026.

https://doi.org/10.1021/jacs.6c00684
J. Am. Chem. Soc. 2026, 148, 18903−18918